N. Slavinskaya[1], M. Abbasi[1], J.-H. Starcke[1], R. Whitside[1], A. Mirzaeva[1], U. Riedel[1], W. Li[2], J. Oreluk[2], A. Hegde[2], A. Packard[2], M. Frenklach[2], G. Gerasimov[3], O. Shatalov[3]; Development of an UQ-Predictive Chemical Reaction Model for Syngas Combustion, Energy & Fuels, 31 (2017) 2274–2297.

Development of an UQ-Predictive Chemical Reaction Model for Syngas Combustion

Journal:	*Energy & Fuels*
Manuscript ID	Draft
Manuscript Type:	Article
Date Submitted by the Author:	n/a
Complete List of Authors:	Slavinskaya, Nadja; DLR Stuttgart, Stuttgart, Germany, Combustion technology Abbasi, Mehdi; Deutsches Zentrum fur Luft und Raumfahrt, Institute of Combustion Technology Starcke, Jan; Deutsches Zentrum fur Luft und Raumfahrt, Institute of Combustion Technology Whitside, Ryan; Deutsches Zentrum fur Luft und Raumfahrt, Institute of Combustion Technology Mirzaeva, Aziza; Deutsches Zentrum fur Luft und Raumfahrt, Institute of Combustion Technology Riedel, Uwe; Institute of Combustion Technology, IWGerman Aerospace Center (DLR) Li, Wenyu; University of California Berkeley, Mechanical Engineering Oreluk, James; University of California Berkeley, Mechanical Engineering Hegde, Arun; University of California Berkeley, Mechanical Engineering Packard, Andrew; University of California at Berkeley, Department of Mechanical Engineering Frenklach, Michael; University of California, Mechanical Engineering Gerasimov, Gennady; Moscow State University, Institute of mechanics Shatalov, Oleg; Moscow State University, Institute of Mechanics

Development of an UQ-Predictive Chemical Reaction Model for Syngas Combustion

N. A. Slavinskaya,*[,†] M. Abbasi,[†] J. H. Starcke,[†] R. Whitside,[†] A. Mirzayeva,[†] U. Riedel,[†] W. Li,[‡] J. Oreluk,[‡] A. Hegde,[‡] A. Packard,[‡] M. Frenklach,*[,‡] G. Gerasimov,[§] and O. Shatalov[§]

[†]German Aerospace Center (DLR), Institute of Combustion Technology, 70569, Stuttgart, Germany
[‡]Department of Mechanical Engineering, University of California, Berkeley, CA 94720, USA
[§]Institute of Mechanics, M. V. Lomonosov Moscow State University, 1 prosp. Michurinskii, Moscow, 119192, Russia

ABSTRACT

An automated data-centric infrastructure, Process Informatics Model (PrIMe), was applied to validation and optimization of a syngas combustion model. The Bound-to-Bound Data Collaboration (B2B-DC) module of PrIMe was employed to discover the limits of parameter modifications based on the systematic uncertainty and consistency analysis of the model-data system, with experimental data including shock-tube ignition delay times and laminar flame speeds. Existing syngas reaction models are reviewed and the selected kinetic data are described in detail. Empirical rules were developed and applied to evaluate the uncertainty bounds of the literature experimental data. The initial H_2/CO reaction model, assembled from 73 reactions and 17 species, was subjected to a B2B-DC analysis. For this purpose, a dataset was constructed that included a total of 167 experimental targets and 55 active model parameters. Consistency analysis of the composed dataset revealed disagreement between models and data. Further analysis suggested that removing 45 experimental targets, 8 of which were self-inconsistent, would lead to a consistent dataset. This dataset was subjected to a correlation analysis, which highlights possible directions for parameter modification and model improvement. Additionally, several methods of parameter optimization were applied, some of them unique to the B2B-DC framework. The optimized models demonstrated improved agreement with experiment, as compared to the initially-assembled model, and their predictions for experiments not included in the initial dataset (i.e. a blind prediction) were investigated. The results demonstrate benefits of applying the B2B-DC methodology for developing predictive kinetic models.

1. INTRODUCTION

Developing predictive reaction models for complex chemical systems requires integration of large amounts of theoretical, computational, and experimental data collected by numerous researchers. The model fidelity is judged by its prior information—the quality of chemical kinetic data used (e.g., models developed from "first principles", with minimal parameter fitting, are favorable) and from posterior information—comparison of the model predictions with available experimental observations. Usually, the latter information is used by researchers for model validation and modification.

In cases of large disagreement between simulations and experimental data, the chemical kinetic parameters are modified to reduce this disagreement and thereby increase the model's quality. The key questions in such a situation are: Should this disagreement be resolved through kinetic parameter modification? Will this model be developed from "first principles"? To address these questions, we must first quantify the uncertainties in the data. It is beneficial to employ multiple data sets collected by different research groups, select objective numerical criteria defining "success", and identify limits for parameter modifications.

The present work reports the results of applying an automated data-centric infrastructure, Process Informatics Model (PrIMe),[1–3] to validate the H_2/CO oxidation reaction model, which is a part of the DLR hydrocarbon reaction mechanism and database.[4,5] The development of reaction models for larger hydrocarbons may require modification of the H_2/CO system, and such modifications must be guided by rigorous mathematical protocols to maintain the physical nature of the reaction model. In light of this, the ultimate aim of the present study was not just to match the experimental data of the H_2/CO system, but to evaluate the feasible set of its kinetic parameters. Bound-to-Bound Data Collaboration (B2B-DC)[2,3,6–11] was employed to discover the actual limits for parameter modifications based on the systematic uncertainty and consistency analysis of the model parameters and related experimental data (ignition delay times and laminar flame speeds). The B2B-DC methodology quantified the degree of consistency between model and data, exposing what we suggested to be the deficiency of the instrumental models of shock-tube experiments.

The manuscript is organized as follows. In Section 2 we review syngas model development, focusing on work performed in recent years. Section 3 presents a brief overview of B2B-DC, which provides the foundation for the analyses described in the paper. We then proceed, in Section 4, with a description of the reaction model, experimental targets, and their associated uncertainties. Presentation and discussion of the numerical results is given in Section 5. We conclude with Section 6, summarizing the present experience and suggesting further directions for improving the predictive ability of modeling syngas combustion.

2. EXPERIMENTAL DATA

A mixture of hydrogen and carbon monoxide (commonly called synthesis gas or syngas) can be obtained from natural gas, coal, petroleum, biomass and even organic waste. Syngas is used as a direct fuel for clean combustion in electricity generation from coal, petroleum coke or heavy residuals in an Integrated Gasification Combined Cycle (IGCC). In recent years, the role of syngas in sustainable combustion processes and promising syngas utilization for power generation triggered further characterization of the H_2/CO combustion system. In kinetic modeling, the H_2/CO oxidation chemistry is the principal building block in the hierarchy of hydrocarbon oxidation models. As a consequence, a large amount of thermo-kinetic and experimental data have appeared for this sub-

system in recent years.[1,4,5,12–112] Table 1 contains the most established, from our point of view, H_2/CO reaction models with experimental validation data that have been collected.

One of the early investigations of H_2/CO chemistry, which underlies most modern models, is the study of Yetter, Dryer and Rabitz.[14] In their study,[14] previous investigation results were analyzed and integrated in a $CO/H_2/O_2$ reaction mechanism, which was tested against a wide range of available experimental data obtained from shock tube and flow reactors,[34–36] Table 1. The model was validated over a combined temperature range of 823 – 2870 K, fuel-oxidizer equivalence ratios φ = 0.5 – 6.0 and pressures p = 0.3 – 2.2 atm. The kinetics were analyzed in three temperature regimes (low, intermediate, and high) where different reaction sets control the radical pool. The high-temperature regime is associated with the H, O and OH radicals while the low temperature regime is dominated by HO_2 and H_2O_2. The intermediate temperature regime serves as a transition zone, in which the concentrations of H, O, OH, HO_2 and H_2O_2 intermediates are all nearly the same order of magnitude. Moreover, this regime embodies the explosion limits, which separate the slow reaction (chain propagation) from the fast reaction (chain branching). Consequently, system pressure and composition affect the limits of these regimes. Uncertainties in the kinetic and thermochemical parameters were analyzed.

The updated H_2/CO subset of the Leeds methane oxidation mechanism[13] implements reaction kinetic and thermodynamic data along with the results (at the time of publication) from H_2/air and wet CO/air combustion mechanisms. The updated mechanism was tested against hydrogen oxidation and H_2/CO oxidation experiments,[37–45] Table 1. Uncertainties of the simulation results, caused by the uncertainties in the kinetic parameters and the heats of formation, were analyzed.

Table 1. Kinetic Models and Validation Data

mechanism	ignition delay	laminar flame speed	JSR	PFR	flame conditions	shock tube conditions
$CO/H_2/H_2O/O_2/N_2/Ar$ Yetter et al., 1991[14]	p = 1.2–2.2 atm T_5 = 2050–2870 K ϕ = 1.6–6.0[34]			p = 0.5–1.0 atm T = 823–1130 K ϕ = 0.5, 1[35,36]		
H_2/air and wet CO/air Zsély et al., 2001, 2005[13]	$H_2/CO/O_2/Ar$ p = 1.4–2.2 atm T_5 = 1400–2870 K ϕ = 0.4[37]	H_2/air, CO/H_2/Air p = 1.0 atm T_0 = 298 K ϕ=0.3–6.6[38–45]				
$CO/H_2/O_2$/air Davis, et al.,2005[15]	p = 1.24–2.2 atm T_5 = 2050–2870 K ϕ= 6.0[34]	p = 1.0 atm T_0 = 298 K ϕ = 0.6–6[45,46]		p = 1.0–9.6 atm T = 960–1200 K ϕ= 0.33–2.1[47]		
$CO/H_2/H_2O/O_2$/Ar/He Saxena et al.[16,17]	p = 0.15–0.3 atm p = 1.4–2.2 atm T_5 = 1400–2870 K ϕ = 0.4, 6.0[34,37]	p = 1.0 atm T_0 = 298 K ϕ = 0.6–6[45,48]				
$CO/H_2/O_2$//H_2O/Ar/air Li et al., 2007[18]	p = 0.15–2.2 atm T_5 = 1400–2850 K ϕ= 0.4–6.1[34,37]	p = 1.0 atm T_0 = 298 K ϕ = 0.6–6[45,49]		p = 1.0–9.6 atm T = 960–1200 K ϕ = 0.33–2.1[35,47,50]		
$CO/H_2/O_2/H_2O$/Ar/air Chaos et al., 2007[19] Updated[18]	p = 50 atm T_5 = 1044 K ϕ = 0.5–1[51]					p = 24–450atm T_5 = 1044–1456 K ϕ = 0.5–1[52]
$CO/H_2/H_2O/O_2$/Ar/He/N_2 Sun et al., 2007[20]	p = 0.1–10.0 atm T = 600–1100 K ϕ= 0.4, 6.0[53] counter-flow	p = 1–40 atm T_0 = 292–700 K ϕ = 0.6–5[20]		p = 1 atm T = 1033, 1034 K ϕ = 0.33–2.1[35]		
$CO/H_2/CO_2/H_2O/O_2$/Ar/N_2/He Frassoldati et al., 2007[21]	p = 1.05–15.0 atm T_5 = 890–2850 K ϕ= 0.5–11.6[34,52,54,55] p = 1.0 atm T = 600–2000 K[53] counter-flow	p = 1.0–10 atm T_0 = 298 ϕ= 0.3–6.6[20,45,46,56–59]	p = 1 atm T_0=850–1350 K ϕ=0.1–2[60]	p = 1.0–9.6 atm T = 960–1200 K ϕ=0.33–2.1[35,47,61,62]	p=0.0395atm T_0= 300 K ϕ= 1.19[63]	p = 256, 450 atm T_5=1044–1456 K ϕ=0.5–1[52]
$CO/H_2/CO_2/H_2O/O_2$/Ar/air/He	p = 1–2.2	p = 1–20 atm	p = 1.0	p = 1.0 atm	p = 0.0526	p = 24.0–43.0

Le Cong et al., 2008[22]	T_5 = 850–1350 K ϕ = 0.6–6[54]	T_0 = 292–700 K ϕ=0.6–5[20,45,64,65]	atm T_0= 850–1400 K ϕ = 0.1–2[60]	T = 1032–1041 K ϕ = 0.5, 1[14,47,48]	atm T_0 = 328 K ϕ = 0.13[63]	atm T_5=1044–1456 K ϕ=0.5–1[52]
$CO/H_2/CO_2/O_2$/air Cavaliere et al., 2010[23]	p = 1.0, 15.0 atm T_5 = 600–1300 K, ϕ = 0.5[67–69]					
$CO/H_2/O_2/N_2$/Ar/He Kéromnès et al., 2013[24]	p = 8–70 atm T_c = 914–1968 K ϕ = 0.5–1.0[24] rapid compression machine	p = 1–10 atm T_0 = 298 K ϕ = 0.5–4[20,45,57,64,65,70–73]				p = 1–32 atm T_5 = 870–2220 K ϕ = 0.5–1.0[24,73] p = 5–10 atm T_5 = 298 K ϕ = 0.5–3.5[24]
$CO/H_2/O_2/N_2$/He Goswami et al., 2014[25]	p = 1–16 atm T_5 = 870–2220 K ϕ = 0.5[24]	p = 1–9 atm T_0 = 298 K ϕ = 0.5–5[20,24,45,65,70,72,73]		$CO/O_2/H_2O/N_2$ p = 1 atm T = 1033 K ϕ = 0.33–2.1[35]		
$CO/H_2/O_2/N_2$/He/Ar/CO_2/H_2O Nilsson & Konnov, 2016[26]	p = 1–20 atm T_5 = 900–1250 K ϕ = 0.3–1.5[67,74]	p = 1–40 atm T_0 = 298–500 K ϕ = 0.5–4.3[20,70,75–82]		p = 1–9.6 atm T = 880–1380 K ϕ = 0.5–2.0[35,47,83]		p = 24–450 atm T_5 = 1100–1475 K ϕ = 1.0[52]
$CO/H_2/O_2/N_2$/He/Ar/CO_2/H_2O Varga et al., 2016[27]	p = 0.8–33.0 atm T_5 = 900–2870 K ϕ = 0.5-6.0[67,68,74,84–87]	p = 0.95-40.0 atm T_0 = 295–600K[20,25,45,46,49,56–58,64,65,70–72,75–79,82,89–96,98–100,113]	p = 1.0 atm T_0= 850–1400 K ϕ = 0.1–1.0[60]	p = 1.0–9.6 atm T = 943–1140 K ϕ = 0.004–1.438[14,47,50,101] p = 1.05 atm T_0 = 795–1450 K ϕ = 0.0005–3[61,62]		p = 21–450 atm T_5 = 995–1495 K ϕ = 0.5–1.0[52]
$CO/H_2/O_2/N_2$/He/Ar/CO_2/H_2O DLR-SynG 2016, pw	p = 0.6–50.0 bar T_5 = 800–2012 K ϕ = 0.5–1.5[51,67–69,73,74,86,102–106]	p = 1.0–40.0 bar T_0 = 300–700 K[20,25,33,45,57,65,75,80,81,90,97,99,107–112]	p = 1.0 atm T_0= 850–1400 K ϕ = 0.1–1.0[60]	CO/O2/H2O/N2 p = 1 atm T = 1033 K ϕ = 0.33–2.1[35]		

Davis et al.[15] proposed a H_2/CO kinetic model based on the GRI-Mech 3.0 model.[114] They presented a comprehensive literature review of kinetic data and performed model optimization within the uncertainty bounds of the relevant rate parameters with respect to 36 targets: experimental data for ignition delays, laminar flame speeds, and species profiles of H_2 and CO measured in flames and flow reactors.[34,45–47] Their model[15] predicts the observed H_2/CO oxidation experimental data over the combined range of T = 298 – 2870 K, φ = 0.33 – 6.0, and p = 1.0 – 9.6 atm (Table 1).

Saxena and Williams[16] tested a relatively small detailed mechanism for propane combustion[17] to predict hydrogen and carbon monoxide combustion. The performed study resulted in the revision of some rate parameters, the elimination of one initiation step in the hydrogen oxidation mechanism, and the addition of an initiation step for carbon monoxide oxidation. With these alterations, a reasonable agreement was obtained with measured burning velocities, diffusion-flame extinction conditions (for H_2/O_2), and auto ignition times,[34,37,45,48] Table 1. Combined parameter ranges were: temperature of 298 K, 1400 – 2870 K, φ = 0.4 – 6.0, pressures p = 0.15 – 2.2 atm.

Li et al.[18] and Chaos et al.[19] updated the model used in the study.[14] Li et al.[18] revised the H_2/CO sub-mechanism in a reaction model for $CO/H_2O/H_2/O_2$, CH_2O and CH_3OH oxidation and modified it based on the published measured data for ignition delays, laminar flame speeds, and plug-flow concentrations profiles,[34,35,37,45,47,49,50] Table 1. Modifications of reaction rate coefficients responsible for the formation of CO_2 and CO were extensively investigated and optimized with weighted least-square fits of available experimental measurements. This resulted in significantly closer prediction of the experimental observations. Chaos et al[19] investigated important features of H_2/CO combustion at high pressures and relatively low temperatures, and also effects of surfaces, trace impurities,

and contaminants. The paper reviewed experimental efforts in the high-pressure syngas oxidation and discussed the kinetic changes proposed in literature for improving predictions of new data. Further H_2/CO kinetic improvements related to investigations[14,18] were also proposed based on recent high-pressure experimental observations,[51,52] Table 1, and associated theoretical works. The authors noted the need for careful analysis of data collected at high pressures.

Sun et al.[20] developed a kinetic mechanism to model the measured laminar flame speeds for CO/H_2/air and CO/H_2/O_2/He mixtures at different equivalence ratios and pressure up to 40 atm. The rate coefficient of reaction CO + HO_2 → CO_2 + OH was calculated based on *ab initio* quantum chemistry and canonical transition state theory. The elaborated mechanism was successfully used to model the experimental data,[20,35,53] Table 1.

Frassoldati et al.[21] extended the previous kinetic model of Ranzi et al.[115] They revised and validated a detailed kinetic model of H_2/CO combustion with a particular focus on NO_x formation and especially on the interactions of the syngas system with nitrogen species.[21] Their paper offers a critical collection of experimental data[20,34,35,45–47,52,54–63] and a kinetic model capable of simulating the combustion of syngas mixtures and the formation of pollutant species across a wide range of conditions, with particular emphasis on high pressures, Table 1.

A syngas mechanism proposed by Le Cong et al.[22] is the H_2/CO sub-model of the detailed combustion kinetic model for H_2/CO/CH_2O/CH_3OH/CH_4 systems. Their updated kinetic scheme was successfully validated against a large set of data for CO and H_2/CO combustion,[14,20,45,47,48,52,54,60,63–65] Table 1. The effects of total pressure, equivalence ratio, and H_2/CO concentrations on flame speeds are well predicted. Also, the kinetics of oxidation of CO and H_2/CO in a turbulent flow reactor, a JSR, and the high-pressure shock tube experiments were successfully reproduced.

Cavaliere et al.[23] adapted Saxena and William's mechanism[16] to intermediate pressures based on the experimental measurements,[67–69] Table 1. The H_2/CO mechanism was tested over a temperature range of 600 – 1400 K and a pressure range of 1.0 – 15.0 atm. H_2O_2 + M= OH + OH + M and H + H_2O_2 = HO_2 + H_2 reactions were found to be the rate-controlling steps for the prediction of the ignition time at high pressures and low temperatures.

A detailed H_2/CO/O_2 reaction mechanism of Kéromnès et al.[24] is based on the former H_2/O_2 mechanism of Ó Conaire et al.[28] with some updates to reflect new experimental data obtained in this work. The reaction sequence H_2 + HO_2 = H + H_2O_2 followed by H_2O_2 (+M) = OH + OH (+M) was found to play a key role in the hydrogen ignition under high-pressure and intermediate- to high-temperature conditions. At low pressures (of the order of 1 atm) and low temperatures (below 1000 K), the process is controlled by the competition between the chain-branching reaction H + O_2 = O + OH and the chain-propagating reaction H + O_2 (+M) = HO_2 (+M). The mechanism accurately reproduces new high-pressure experimental data (ignition delay times and flame speed) relevant to gas-turbine conditions[24] as well as previous experimental data.[20,24,45,57,64,65,70–73]

The H_2/CO kinetic mechanism of Goswami et al.[25] is based on the H_2/O_2 mechanism of Konnov[29] and includes recently evaluated rate coefficients. The CO set of reactions was taken from Konnov 0.6 version[30] with few modifications. After validation against new measurements, the kinetic mechanism was further validated using experimental data available in the recent literature for lean and rich mixtures at elevated pressures. These data included laminar burning velocities,[20,24,45,65,70,72,73] ignition delay times,[24] and speciation measurements.[35]

The kinetic mechanism of Nilsson and Konnov[26] is a further expansion of the H_2/O_2 mechanism recently proposed by Alekseev et al.[31] The reaction rate coefficients were chosen based on an extensive literature review. Particular attention in this mechanism was given to the chemistry of HOCO, produced from the CO+OH reaction. It must be pointed out that most available syngas mechanisms do not include HOCO since it is only expected to be of importance at some extreme high-pressure and low-temperature conditions. The mechanism was validated against a wide range of experimental data including ignition, flame structures, and laminar flame speeds,[20,35,47,52,67,70,74–83] with particular attention given to laminar burning velocities. Variations in the H_2/CO ratio, pressure, temperature, and diluents (CO_2, H_2O, and N_2) were considered. In comparison with the mechanism of Kéromnès et al.,[24] this mechanism gives better agreement with experimental laminar burning velocities at rich conditions.

Varga et al.[27] developed an optimized joint hydrogen and syngas combustion mechanism. The model of Kéromnès et al.[24] was updated with the recently optimized hydrogen combustion mechanism of Varga et al.[116] and further optimized using a global parameter optimization method.[117] The experimental data included ignition delay times measured in shock tubes and rapid compression machines (1723 targets, 156 data sets), burning velocity measurements (2311 targets, 256 data sets), and species profiles measured in shock tubes, flow reactors (968 targets, 53 data sets), and jet-stirred reactors (103 concentration targets, 11 data sets). Directly measured rate coefficients of 15 reactions were also utilized. 48 Arrhenius parameters and five third-body collision efficiencies of 18 elementary reactions were optimized. The optimized mechanism was compared to 19 recent hydrogen and syngas combustion mechanisms and was shown to provide the closest reproduction of the used experimental data.

The experimental data applied for model validation in the present study are listed in the last row of Table 1 and in Tables S1 and S2 of Supporting Information. Only ignition delays and laminar flame speeds were used in the analysis: these experimental measurements generally have lower uncertainty in comparison to species concentration profiles. Also, the quantity of experimental ignition-delay and laminar-flame-speed measurements greatly exceeds those of species concentrations. Having more data included in the analysis should provide more objective statistics and more meaningful model validation.

The importance of uncertainty in chemical-kinetics problems prompted development of methods for kinetic model optimization and uncertainty quantification.[2,3,6–11,117–120] In the present work, we utilized the methodology of Bound-To-Bound Data Collaboration (B2B-DC),[2,3,6–11,117–120] which is briefly described next. We then proceed with a description of the newly-constructed dataset, i.e., the selected experimental targets, reaction model, and associated uncertainties, detailing the methodology adopted for evaluation of the uncertainties. This will be followed by presentation and discussion of the numerical results.

3. THEORETICAL BACKGROUND: BOUND-TO-BOUND DATA COLLABORATION (B2B-DC)

B2B-DC is an optimization-based framework for combining models and experimental data from multiple sources to explore their collective information content.[2,3,6–11,119,120] The approach can decisively indicate whether related experimental data are consistent with each other within a specified chemical kinetics model, explore sources of inconsistency, discriminate among differing models, make model interval predictions, and analyze sensitivity of uncertainty propagation. We begin by reiterating some key definitions.

Quantities of Interest (QoI) is a collection of experimental observations of physical processes, coupled with respective uncertainties, assessed as lower and upper bounds on the observed values, i.e., L_e and U_e for each e-th QoI. Each physical process can be represented by a common chemical-reaction model, $C(x)$, and a reactor-physics model, R_e, the two forming a combined numerical model that we refer to as $M^e(x)$, with prior knowledge on the domain of parameters thus constraining each parameter x to an interval $[x_{min}, x_{max}]$ and all together to a hypercube $x \in \mathrm{H}$.

A key requirement for B2B-DC is the formulation of a *dataset*, which entails creation of dataset units for all QoI, $e = 1, 2, \ldots$, from a common kinetic model, experimental observations, and their uncertainties.

The computational model $M^e(x)$ must produce outputs that are consistent with the reported QoI uncertainties. Hence additional constraints that the true model parameters must satisfy are

$$L_e \le M^e(x) \le U_e \quad \text{for all } e. \tag{1}$$

The subset of H satisfying (1) is called the *feasible set*, F, of parameters, i.e., all model parameter values that jointly satisfy all of the prior information and all their model predictions are consistent with the reported experiment observations. The integral part of the B2B-DC framework is approximation of the $M^e(x)$ outputs for given QoI by quadratic (or rational quadratic) surrogate models,[10] $M_e(x)$,and hence the feasible set can be define as

$$\mathrm{F} := \{x \in \mathrm{H}: L_e \le M_e(x) \le U_e \quad \forall e\} , \tag{2}$$

where $M_e(x)$ designates a surrogate model of e-th QoI. A parameter value that is not in F is at odds with at least one of these constraints.

In this way, the first "bound" in the "bound-to-bound" nomenclature is associated with (a) the form of the prior information, namely that the true model parameters must be both contained in the parameter hypercube H (in the form of bounds on the components), and (b) the true parameters must result in model predictions of all QoI (i.e., training experiments) that are within the measurement bounds declared by the experimenters, namely $L_e \le M_e(x) \le U_e$ for all e. Together, these are the "bounds" that define F. Subsequent B2B-DC computations (model parameter analysis and optimization) can be performed only if the feasible set F is non-empty.

Dataset consistency is analysis that examines the existence of a feasible parameter vector by determining the consistency measure of dataset D,[7]

$$\begin{aligned} C_{\mathrm{D}} &= \max_{\gamma, x \in \mathrm{F}} \gamma, \quad \text{subject to (for all } e\text{):} \\ &(1-\gamma)\frac{L_e - U_e}{2} \le M_e(x) - \frac{L_e + U_e}{2} \le (1-\gamma)\frac{U_e - L_e}{2} \end{aligned} \tag{3}$$

In this definition, the original constraints (1) are augmented with a scalar relaxation parameter, γ, where positive values of γ imply tightening of the constraint (dataset is consistent) and negative values imply loosening (dataset is inconsistent). The consistency measure, C_{D}, quantifies how much the constraints can be tightened while still ensuring the existence of a set of parameter values whose associated model predictions match (within the bounds) the experimental QoI.

Model prediction is the prediction interval for property P by model M_P that is consistent with all of the model/observation pairs in the dataset. The B2B-DC computation expresses that into two optimization problems for the lower and upper interval endpoints, L_P and U_P,

$$L_P := \min_{x \in F} M_P(x)$$
$$U_P := \max_{x \in F} M_P(x) \quad (4)$$

The length $U_P - L_P$ quantifies the amount of uncertainty in M_P's value conditioned on the fact that the true parameter vector is contained in the feasible set F. The mathematical methodology of B2B-DC is invoked for the constrained optimization of a function of interest f over the feasible set F. The computed f_{min} and f_{max} constitute the "to-bound" aspect: the bounds that describe the prior information and the bounds on experimental observations are mapped into bounds on prediction. The mathematical details for polynomial surrogate models can be found in Seiler et al.[11]

In what follows, a consistent dataset for the studied H_2/CO data-model system will be produced and tested for consistency. The kinetic model will be optimized over the feasible region of the parameter space of the H_2/CO data-model system using methods described in You et al.[120] Optimization constrained to the feasible set, methods LS-F and 1N-F,[120] ensures that all model predictions fall within the uncertainties of experimental QoI. Method LS-F uses a weighted least-squared objective, while 1N-F is a one-norm minimization that aims at the smallest *number* of parameters to be changed. We also employed, for comparison, method LS-H, which is a least-squared minimization constrained to the prior-knowledge hypercube, H.

4. DLR-SynG DATASET

A key requirement for the analysis is the formulation of a dataset, which entails creation of dataset units from experimental observations and a common kinetic model. A dataset unit consists of the measured observation, uncertainty bounds on the measurement, and a model that transforms active parameter values into a prediction for the measured QoI. Active parameters were identified via sensitivity analysis.[10] A quadratic response surface was developed for each QoI in terms of its own set of active parameters via computer experiments performed by sampling x from H, arranged to a factorial design.[10] Once developed, the dataset can be subjected to rigorous numerical analysis.

4.1. Ignition-delay-time QoI. To account for syngas ignition, we selected a set of the shock-tube syngas ignition measurements[51,67–69,73,74,86,102–106] that covers a wide range of temperatures (800–2500 K), pressures (0.5–50 bar), and equivalence ratios (φ = 0.5–1.50). Evaluation of L_e and U_e for each QoI was accomplished by creating an empirical rule which is motivated below.

The fuel ignition produced in a shock tube is a combination of several physical and chemical phenomena. Fluid-flow patterns developed behind the shock that cannot be assumed homogeneous and uniform are classified as "non-idealities" of shock-tube experiments.[103,121–129] Facility-dependent effects and energy-release phenomena can increase the non-idealities and influence the instrument readings, thus adding to the uncertainty of experimental data. Although the presence of the non-idealities in shock tubes have been well-documented,[103,123–130] there are no simple protocols to quantitatively assess their impact on measured ignition delays. And yet, it is this assessment that may determine the usefulness of the experimental data for model validation. The issue is not just a few percent

uncertainty in the measured value, but realization that the observed phenomenon can be an expression of mechanisms other than chemical kinetics. The origin of such a conclusion goes to the work of Tony Oppenheim, who introduced distinction between *mild* and *strong* ignition,[130] the latter is driven essentially by chemistry but the former is not. The results of the present study, supported by a rigorous quantitative assessment, point further to the paramount importance of considering such aspects for suitability of QoI selection for model validation. We will return to this point later in the text.

In the present study, we designed an empirical algorithm for a priori assignment of the uncertainty bounds to the measured observations included in the dataset. For this purpose, the strongest non-ideality phenomena were determined across the investigations and the facility-related and fuel-related factors that affect these phenomena were identified. The dominant non-ideality phenomena were attributed to two gas-dynamics effects: i) boundary layer formation after shock passing (resulting in hydro- and thermo-inhomogeneities behind the shock-wave); ii) post-shock compression (interaction of the reflected shock-wave with the contact surface). The factors which influence these phenomena are: operating conditions, length and diameter of the driven section, duration of the reaction, mixture dilution, and nature of carrier gas (CG).

The systematic experimental uncertainty (affected by temperature, pressure, and concentration measurements, as well as by measurement location) was estimated to be 15 %. The "ideal case" (vanishing influence of "non-idealities") was defined as measurements performed in a shock tube with the driver-section length ≥ 3.0 m and the driven-section length ≥ 8.0 m with an internal diameter (most important factor) larger than 10.0 cm, in a temperature interval of 1000-1600 K, pressure less than 15 atm, a fuel-air ratio exceeding 0.3, dilution with a monoatomic gas 1:2 or higher, and the measured ignition delay time t_{meas} lower than 500 μs.[103,123–129] Deviations from these conditions were evaluated by adding a 5 % uncertainty for each criterion not satisfied to the ideal case. For measured ignition delay time longer than 1000 μs, a 5 % uncertainty was added per every 500 μs. Radical impurities were evaluated as extra 5 % uncertainty. The resulting uncertainty evaluation is documented in Table 2. Ignition delay targets selected for analysis and their evaluated uncertainties can be found in Tables S1 and S3 of Supporting Information.

Table 2. Evaluation of Uncertainty Intervals for Selected Shock-Tube Experiments; the Starting Uncertainty is 20 %

driven-section dimensions				temperature interval (K)		pressure (atm)		dilution		t_{meas} (μs)	
length (m)		internal diameter (cm)									
>8		>10		T<1000	+5%	P>15	+5%	yes		0-50	+5%
<8	+5%	<10	+5%	T>1600	+5%	P>30	+10%	none (air)	+5%	50-500	+0%
						every 15	+5%			500-1000	+5%
										1000-1500	+10%
										every 500	+5%

4.2. Laminar-flame-velocity QoI. To represent flame-propagation conditions, we selected a set of flame velocities at 0.1–0.5 MPa that have been investigated by using a variety of techniques, Table 1. The laminar flame speeds included in the present dataset were taken from studies,[20,25,33,45,57,65,75,80,81,90,97,99,107–112] Table S2 of Supporting Information. They were selected to cover the full range of operating conditions available in the literature. The flame speeds measured at high pressures are relatively scarce. Experimentalists estimate the current uncertainties in laminar flame speed measurements to be in a range of about 5–10 %, increasing with pressure

(>0.5 MPa) and fuel-air ratio ($\varphi > 2$). Figure 1 shows the uncertainty bars adopted from literature[73] for atmospheric conditions. From our evaluation of the available data, illustrated in Figure 1, the uncertainty of syngas atmospheric laminar flame speeds can be assumed to be 10 % for $\varphi < 2$, 15 % for $2 < \varphi < 3$, and 20 % for $\varphi > 3$. For higher pressures, we added 5 % to the uncertainty. The results of this empirical rule for the data uncertainty evaluation are reported in Table 3. Laminar flame speed targets selected for analysis and their evaluated uncertainties can be found in Tables S2 and S4 of Supporting Information. The complete dataset contains 167 QoI, 122 ignition delays and 45 laminar flame speeds, presented in the Supporting Information.

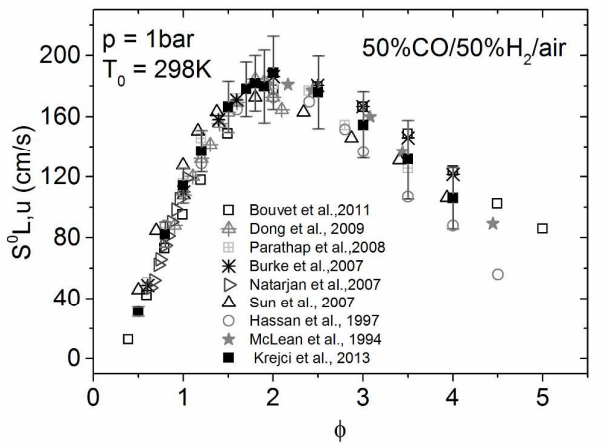

Figure 1. Comparison of literature experimental data[73] for atmospheric 50:50 H_2/CO/air laminar flame speed with the reported uncertainty bars.[73]

Table 3. Evaluation of Uncertainty Intervals for the Selected Laminar Flames

φ	p (atm)	error (%)	p (atm)	error (%)	p (atm)	error (%)
0.5–2	1–5	10	5–10	15	>10	20
2–3	1–5	15	5–10	20	>10	25
>3	1–5	20	5–10	25	>10	30

4.3. Kinetic Model. The chemical-reaction model assembled for the studied H_2/CO system (6 elements, 17 species, 73 reactions) is a sub-model of the DLR C_0-C_2 reaction model,[5] which is the base chemistry of the DLR reaction database for heavy-hydrocarbon oxidation. Originally, this kinetic model was based on the H/O, C_1 and C_2 chemistry of the Leeds Methane Oxidation Mechanism;[4,13,131] it has been improved, modified and extended[5] on the basis of experimental data partially integrated in Table 1. The complete list of the involved reactions and their kinetic parameters are reported in Table S5 of the Supporting Information. Most of the used kinetic data follow Baulch et al.'s recommendations.[12] The modifications made in the present study, relatively to prior evaluations,[12,13,131] are discussed next.

The chain initiation reaction

$$H_2 + O_2 \rightarrow OH + OH \qquad (R1)$$

was included in the model in addition to the competing step[12]

$$H + HO_2 \rightarrow H_2 + O_2 \qquad (R2)$$

Literature data involved in the rate coefficients analysis for reaction (R1) are presented in Figure 2. The values from Ripley et al.[132] and Jachimovski et al.[133] were obtained from the rate coefficient optimization of the experimental ignition delays. Karkach and Osherov[134] calculated the rate coefficient for reaction (R1) using transient-state theory and this value was adopted in the model with an uncertainty factor of 10. To support this selection, the comparison of the rate coefficient calculated by Karkach and Osherov[134] for the reverse of reaction (R2) with experimental data obtained in the study[135] is shown on Figure 2.

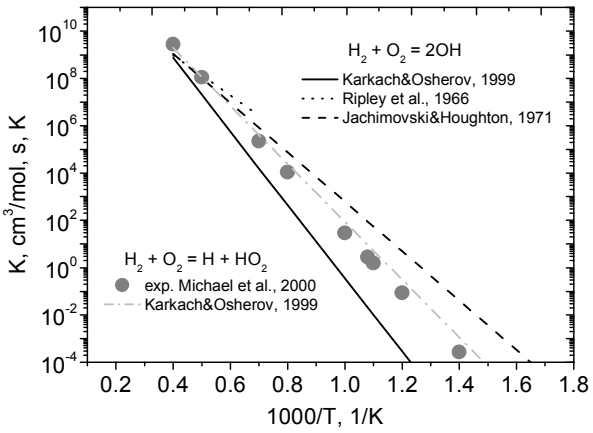

Figure 2. Arrhenius plot of rate coefficients for the $H_2 + O_2 \rightarrow OH + OH$[132–134] and $H_2 + O_2 \rightarrow H + HO_2$[135] reactions.

The three-molecular reaction

$$H + O_2 (+M) \rightarrow HO_2 (+M) \qquad \text{(R3)}$$

strongly influences combustion regimes of hydrogen and can shift the explosion limit behavior of H_2/O_2 mixtures. Hence reaction (R3) has been extensively studied experimentally and theoretically.[29,102,136–141] A significant progress has been made to provide a detailed description of the rate coefficient dependence on temperature, pressure, and chemical nature of the bath gas M. The rate coefficients obtained and recommended in the literature have very similar values, but F_{cent} has a relatively large discrepancy in the data: $F_{cent} = 0.5–0.72$ for M = Ar, N_2 and $F_{cent} = 0.5–0.8$ for M = H_2O.[137,140,141] The rate coefficient of Troe[137] was incorporated in the model for the high-pressure limit. The low-pressure-limit rate coefficients for M = He, O_2, N_2 measured by Michael and co-workers[138] and for M = Ar, H_2O measured by Bates et al.[139] were adopted. The study and recommendations of Fernandes et al.[140] performed for the falloff behavior were considered: $F_{cent} = 0.5$ for M = He, Ar, O_2, N_2 and $F_{cent} = 0.6$ for M = H_2O.

The rate coefficients of hydrogen recombination with different third bodies,

$$H + H + M \rightarrow H_2 + M\,, \qquad \text{(R4)}$$

were updated on the basis of analysis performed in the work.[136] We note that there are no reliable experimental data for this reaction and its reaction rate value accepted in the literature, in different models and reviews, follows from.[142] For M = Ar, the rate value from the study[12] and for M = H, H_2, N_2 and H_2O from the investigation[142] were used in the present model.

The atom transfer reaction

$$CO + O_2 \rightarrow CO_2 + O \quad \text{(R5)}$$

has been studied by different research groups and is well documented.[37,143–147] Selected experimental data are shown in Figure 3. The correlation recommended by Tsang and Hanson[143] and quantum chemical calculations of Sharipov and Starik[144] give good agreement with the experimental data. The rate coefficient adopted in the present work is based on the recommendation of Tsang and Hanson[143] with an uncertainty factor of 5.

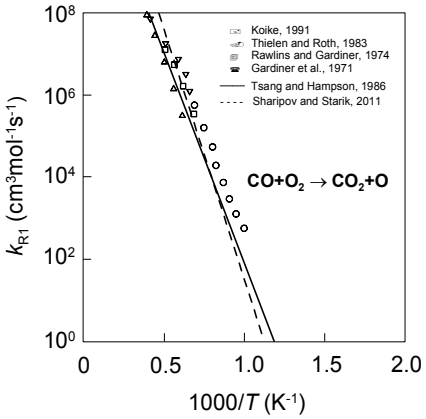

Figure 3. Temperature dependence of the rate coefficient for reaction (R5) measured by different researchers (symbols) and estimated by Tsang and Hampson[143] and Sharipov and Starik[144] (lines).

The bimolecular reaction

$$H + HCO \rightarrow H_2 + CO \quad \text{(R6)}$$

has a chain-terminating character. Three microscopic pathways are identified for this reaction. One is a direct abstraction and the others both proceed via collision complex formation followed by either transition-state-mediated or roaming dynamics. The formation of H_2 and CO at all temperatures occurs predominantly by direct abstraction studied by Christoffel and Bowman.[148] The recommendation of Baulch et al.,[12] adopted in the present study, treats the rate coefficient of this reaction as nearly independent of temperature between 298 and 2500 K, with an average value of 9.0×10^{13} $cm^3mol^{-1}s^{-1}$ and an uncertainty factor of 2. These data agree with relatively new the experiments of Friedrichs et al.[149] and the classical trajectory study of Troe and Ushakov.[150]

The well-studied reaction

$$HO + CO \rightarrow H + CO_2 \quad \text{(R7)}$$

is important in combustion chemistry because it is the main pathway in the conversion of CO to CO_2 with a major energy release derived in the oxidation of hydrocarbons. The reaction rate coefficient is essentially flat at low temperatures but increases quickly at $T > 500$ K.[12] This behavior is attributed to the complex mechanism of the reaction that proceeds via the formation of a vibrationally-excited HOCO intermediate, HOCO*, which can decompose to form H and CO_2 or undergo collisional stabilization. Joshi and Wang[151] showed that the formation of the HOCO adduct leads to an increase in the rate coefficient with pressure, but most available syngas mechanisms do not include HOCO. Recently, the inclusion of the HOCO reaction subset was investigated by Nilsson and

Konnov.[26] It was shown that HOCO reaction subset does not alter the model predictions of laminar burning velocities, ignition delay times or oxidation and can be needed mostly at the high pressures and low temperatures. Therefore, HOCO was not included in the present mechanism and reaction (R8) was treated as pressure independent. Its rate coefficient was based on Baulch et al.'s recommendation,[12] which is in good agreement with recent experimental investigations.[151,152] The uncertainty factor of this rate coefficient was estimated to be 1.26.

High-temperature oxidation of hydrocarbons is known to be sensitive to reaction

$$HCO + O_2 \rightarrow CO + HO_2 \quad . \qquad \text{(R8)}$$

Other channels of this reaction that form CO_2 + OH or HCO_3 are of little importance under the conditions relevant to combustion.[12] Recent shock-tube measurements of Colberg and Friedrichs[153] in the temperature range 739−1108 K and of Fassheber[154] at temperatures of 1285−1760 K allow a reasonable fit of the overall temperature dependence of the available data in the form of an extended Arrhenius expression over the temperature range 295−1705 K, $k_{R8} = 6.92\times10^{6}T^{1.90}e^{690/T}$ $cm^3mol^{-1}s^{-1}$, as shown in Figure 4. This expression was accepted in the present work. The uncertainty of this rate constant is close to a factor of 2.5.

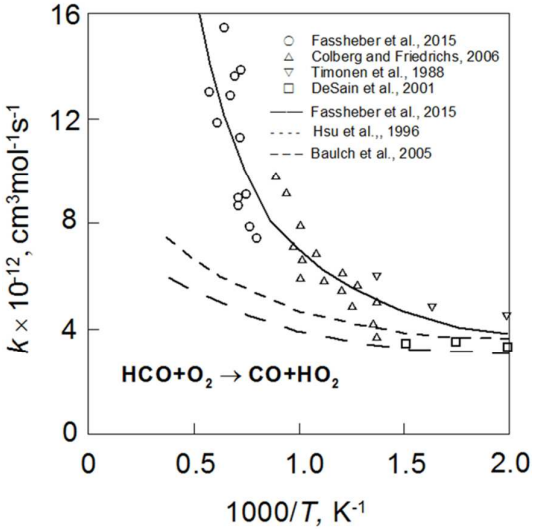

Figure 4. Arrhenius plot of the measured rate coefficient k_{R9} from Colberg and Friedrichs,[153] Fassheber et al.,[154] DeSain et al.,[155] Timonen et al.,[156] the theoretical study of Hsu et al.,[157] and recommendations of Fassheber et al.[154] and Baulch et al.[12]

Although there is much interest in reaction

$$CO + HO_2 \rightarrow CO_2 + OH \qquad \text{(R9)}$$

because of its influence on syngas combustion at high pressure and temperature, large discrepancies exist among literature rate values for gas-turbine operating conditions.[20,50,143,158,159] Existing experimental studies of rate coefficient of reaction (R9) have been performed mostly for low temperatures, below 500 K. At higher temperatures, the rate coefficient has been evaluated either indirectly or inferred from kinetic measurements when reaction (R9) is of secondary importance.[158] In the previous revision of the present model, the reaction rate coefficient was adopted from Tsang and Hampson.[143] It was recently pointed out that the rate should be revised to a lower value. For instance, such a trend was obtained by Mueller et al.[50] in the development of a detailed kinetic

mechanism on the basis of experimentally measured species profiles over wide ranges of pressure (0.5–14.0 atm) and temperature (750–1100 K). The estimations of Mittal et al.[159] deduced from ignition delay measurements and modeling with a complex kinetic model, also suggest a decrease in the rate coefficient by a factor of 10 from that of Baulch et al.[12] Further decrease in the rate coefficient value of reaction (R9) was suggested in *ab initio* calculations performed at pressures up to 40 atm and temperatures 300–2500 K by Sun et al.[20] and for pressures up to 500 atm and temperatures 300–2500 K by You et al.[158] The value of the rate coefficient adopted in our model for reaction (R9) follows the calculations of Sun et al.[20] with an uncertainty factor of 2.

The hydrogen atom in HCO is weakly bonded and is relatively easily lost in direct unimolecular decomposition under combustion conditions

$$HCO + M \rightarrow H + CO + M \qquad (R10)$$

The direct measurements of the rate coefficient for this reaction at moderately low temperatures were performed by Timonen et al.[160] (M = He, N_2, and Ar) and by Krasnoperov et al.[161] (M = He). The data of Friedrichs et al.[149] bridge the temperature gap between Timonen's and Krasnoperov's direct data and the indirect high-temperature measurements of Cribb et al.,[162] as shown in Fig. 5. In the study of Li et al.,[18] the weighted least-squares fit of literature results for reaction (R10) yielded $k_{10} = 4.75\times10^{11} T^{0.66} e^{-7485/T}$ $cm^3mol^{-1}s^{-1}$, which predicts values within uncertainties of both prior and new measurements.[149,155,156,161] It must be pointed that these correlations were obtained by fitting low-pressure-limit data. Nevertheless, significant deviations from the low-pressure limit can occur only at high pressures[161] that are beyond the scope of practical combustion processes.[160] Therefore, reaction (R10) may be regarded as being in the low-pressure limit for most combustion applications. The rate constant adopted in the present work was based on the recommendations of Li et al.[18]

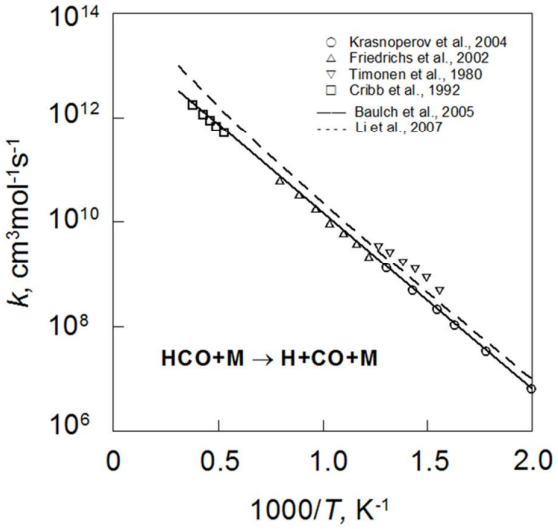

Figure 5. Rate coefficient of reaction HCO + M → H + CO + M. Symbols are experimental data. Lines are the recommendations of Baulch et al.[12] and Li et al.[18]

Destruction of CO by O atoms in reaction

$$CO + O (+M) \rightarrow CO_2 (+M) \qquad (R11)$$

is important only in the dry combustion of CO because the destruction of CO by OH radicals is much faster otherwise. Therefore, a major problem in measuring the rate coefficient of reaction (R11) is that any H_2O impurity leads to OH formation that, in turn, accelerates CO destruction significantly. The rate coefficient exhibits pressure dependence at pressures in excess of 1 atm.[143] Available data show that the activation energy in the low-pressure limit seems to be positive at low temperatures but negative at high temperatures, switching at about 1000 K.[163] In most combustion models,[15,18,24,33] the combination of the low-pressure rate coefficient from Westmoreland et al.[163] and the high-pressure rate coefficient from Troe,[164] slightly modified by Mueller et al.,[50] is used. The rate coefficient adopted in the present work was based on this latter recommendation, with the uncertainty factor of 2. Another recommendation is based on the low-pressure rate constant of Tsang and Hampson.[143] Nilsson and Konnov[26] use the recently calculated high-pressure rate coefficient of Jasper and Dawes,[165] which is 7 to 35 times larger than the value used in many combustion kinetic models.

The present model was extended with OH^* reaction sub-mechanism, taken from Kathrota et al.,[166] to reproduce the ignition delay times recorded in shock tubes by the OH^* chemiluminescent measurements. The active model parameters were multipliers to the rate coefficients, denoted hereafter by λ; they are listed in Table S6 of Supporting Information. The reasoning behind using only multipliers is discussed below, in Section 5.2. The uncertainties in the active parameters, represented by the lower and upper bounds, were assumed equal to those proposed in literature sources or evaluated from a statistical treatment of the literature data.

A preferred key (or PrIMe ID) was prescribed to each structural element in the reaction model. In this way, each structural element has a "pointer" to the referenced information and/or file. Such constructed set of files defines the reaction model, $C(x)$, in PrIMe. All the experimental and model data were documented in the PrIMe Data Warehouse. Selected for analysis experimental QoI are described in the *dataAttribute* files of the PrIMe data collection.[1] These QoI together with the corresponding model $M_e(x)$ and the experimental and parameter bounds form a *dataset*. We will designate the present dataset as DLR-SynG. The complete model and experimental data are available in the PrIMe Data Warehouse.[1]

5. RESULTS AND DISCUSSION

The ignition delay times and laminar flame speeds were modeled with numerical tools of PrIMe[1] and numerical packages CHEMKIN II[167] and Chemical Workbench.[168] The ignition delay time was computationally defined by the peak in the OH or OH* concentration, temperature, or pressure. The thermal diffusion model was applied for calculation of one-dimensional freely propagating laminar premixed flame using CHEMKIN II with over 1000 grid points for each condition.

5.1. Consistency analysis. We began the analysis by employing eq 3 with the initial dataset, DLR-SynG 0, which included all 167 QoI (122 ignition delays and 45 laminar-flame speeds) and 55 active parameters, Tables S3, S4 and S5 of Supporting Information. The results indicated a massive inconsistency. Eight QoI, those listed in Table 4, were found to be self-inconsistent. These were the ignition delay times that were not able to be reproduced within their respective uncertainty bounds by the model employing rate coefficients within their respective uncertainty bounds, H. These eight self-inconsistent QoI were removed from the initially-constructed dataset, thus forming what we refer to as the DLR-SynG 1 dataset. The latter, however, still remained an inconsistent dataset.

Table 4. The 8 Self-inconsistent QoI

T_5 (K)	p_5 (MPa)	φ	target PrIMe ID	estimated uncertainty (%)	ref
1263	0.11	0.5	a00000309	30	[67]
1695	0.16	0.5	a00000352	30	[24]
2004	0.16	0.5	a00000355	25	[24]
1975	0.16	0.5	a00000358	25	[24]
1436	0.16	0.5	a00000359	25	[24]
1027	0.16	0.5	a00000360	35	[24]
1883	0.16	0.5	a00000503	30	[104]
1008	0.16	0.5	a00000504	50	[104]

To continue with the analysis, we employed a newly-developed method of computing the *vector consistency measure* (VCM), similar to eq 3, but with original constraints augmented with *individual* relaxations γ_e for each bound.[169] The VCM method determines the minimal bound changes, each bound by its own extent, that result in dataset consistency. Its application to DLR-SynG 1 identified such a dataset-consistency point by changing 30 ignition delay times and 7 laminar flame speeds, shown in Tables 5 and 6, respectively. We emphasize that the VCM-identified feasible parameter set is a *single point* in H. As this point possesses some optimal attributes, we compare the model predictions obtained with this set of parameters, $M(x_{\mathrm{VCM}})$, to the optimization results in Section 5.3.

To proceed with further features of the B2B-DC framework, we created a new dataset by removing the 37 QoI identified by VCM, thus forming the DLR-SynG 2 dataset contacting 122 QoI. This latter dataset is consistent, meaning that all its 122 QoI are consistent with each other and with the 55 active parameters.

Table 5. Bound Changes of the Ignition QoI Suggested by VCM

T_5 (K)	p_5 (MPa)	φ	target PrIMe ID	estimated uncertainty (%)	reference	lower bound change (%)	upper bound change (%)
900	0.06	0.5	a00000110	50	[67]	-14.84	
936	0.12	0.5	a00000113	40	[67]		13.00
1015	0.11	0.5	a00000189	30	[67]		0.92
1183	0.11	0.5	a00000190	30	[67]		10.14
929	0.26	0.5	a00000191	50	[67]		431.95
1132	1.62	0.5	a00000228	35	[86]	-12.78	
1051	1.53	0.5	a00000236	30	[86]	-2.56	
1097	1.56	0.5	a00000237	35	[86]	-13.48	
1054	1.56	0.5	a00000241	30	[86]		86.11
1057	0.11	0.5	a00000308	30	[67]		1.46
977	0.23	0.5	a00000310	40	[67]		187.12
1149	0.20	0.5	a00000311	30	[67]		28.59
1304	0.17	0.5	a00000312	30	[67]		48.63
943	2.23	0.5	a00000316	35	[68]		175.15
1182	1.20	0.5	a00000335	25	[24]		11.94
1351	0.16	0.5	a00000353	30	[24]		17.76
980	0.16	0.5	a00000354	40	[24]		44.21

1273	0.16	0.5	a00000356	25	[24]		6.02
992	0.16	0.5	a00000357	35	[24]		28.49
1146	0.16	0.5	a00000490	30	[104]	-4.55	
1397	1.25	0.5	a00000498	30	[104]	-16.77	
1284	1.25	0.5	a00000499	30	[104]	-1.25	
1100	1.25	0.5	a00000500	30	[104]		51.79
1360	1.25	0.5	a00000505	30	[104]		51.07
1291	3.20	0.5	a00000507	30	[104]		14.50
981	0.12	1.0	a00000491	20	[106]	-79.93	
1065	0.13	1.0	a00000492	20	[106]	-6.40	
975	0.17	1.0	a00000495	20	[106]	-34.47	
999	0.18	1.0	a00000496	20	[106]	-44.16	
1048	0.17	1.0	a00000497	20	[106]	-10.55	

Table 6. Bound Changes of the Laminar-flame-speed QoI Suggested by VCM

T_0 (K)	P (MPa)	mixture	φ	target PrIMe ID	estimated uncertainty (%)	reference	lower bound change (%)	upper bound change (%)
300	0.10	50/50% CO/H_2/air	0.8	a00000128	10	[20]	-0.73	
300	0.10	50/50% CO/ H_2/air	1.2	a00000129	10	[20]	-0.30	
300	0.10	95/5% CO/ H_2/air	1	a00000260	10	[20]		2.43
300	0.05	95/5% CO/ H_2/air	1	a00000269	10	[57]		4.74
300	0.10	95/5% CO/ H_2/air	0.6	a00000271	10	[57]	-6.75	
600	1.50	50/50% CO/ H_2/He	0.6	x00000471	20	[65]	-6.18	
373	0.10	50%H_2-50%CO/air, H_2O=0.15	1.2	a00000534	10	[81]		5.34

5.2. Posterior Information. The Reader may recall that we started the analysis by creating H, which designates a subset of parameters that represents the prior knowledge on their uncertainties. The shape of H can be either rectangular, implying independence of individual parameter uncertainties,[6,10] or truncated by planes or surfaces imposing known correlations among parameters. Typical examples of such a priori correlations are those between pre-exponential factors and activations energies of rate coefficients[116,117] or rate-constant ratios.[170] While there are no limitations to employing such additional information within the B2B-DC framework, the present results indicate that the main point at issue is the quality of the experimental data and not necessarily that of parameters. This is demonstrated by examining sensitivities of the consistency measure of the DLR-SynG 2 dataset with respect to the uncertainty bounds of parameters and QoI, displayed in Figure 6. Inspection of these results shows a significantly larger impact (i.e., |sensitivity × uncertainty|) on the degree of consistency from the experimental uncertainty as compared to that of the parameter uncertainty. In light of this, we employed a rectangular H in the present work, leaving the a priori parameter correlations to future refinements.

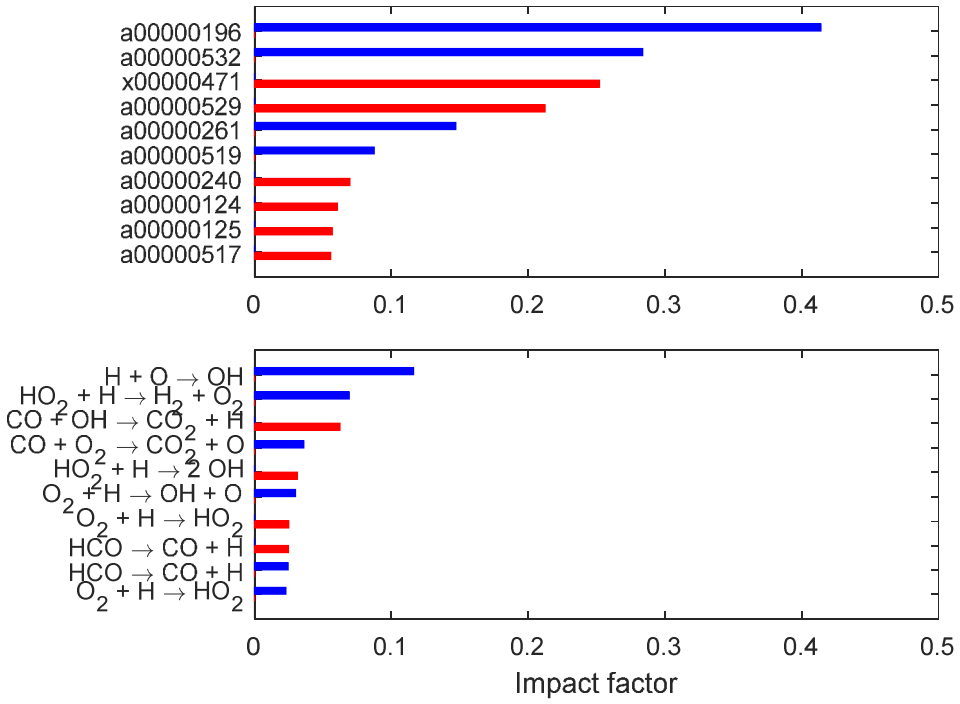

Figure 6. Impact factors of DLR-SynG 2 consistency measure with respect to upper (red) and lower (blue) uncertainty bounds of QoI (top) and model parameters (bottom); only top ten are shown for each case.

While H designates prior information, feasible set F summarizes *posterior* information: all parameter value combinations that satisfy their own bounds and also the QoI bounds. The size and shape of F compared to those of H represent information gained as a result of the B2B-DC analysis. Projection of F on each of the x's yields the posterior range of the parameter uncertainty.[6] Those that changed are reported in Table 7. For the rest of the parameters, the posterior ranges were the same as the prior ones, indicating that the experimental data included in the present analysis did not aid in narrowing down the uncertainty ranges of these parameters *individually*. However, such an outcome does not necessarily imply no information gain for a given parameter: while the extreme parameter values (bounds) may not change, the feasible set may, and usually does, eliminates some combinations of these parameters with others, which is addressed next.

Table 7. Active Parameters with Decrease in Uncertainty Ranges; Bounds that Changed are Shown in Red

reaction	prior bounds		posterior bounds	
	lower	upper	lower	upper
$HO_2+H\rightarrow H_2+O_2$	-0.69	0.69	-0.57	0.69
$CO+OH\rightarrow CO_2+H$	-0.22	0.23	-0.22	0.078
$CO+O(+M)\rightarrow CO_2(+M)$	-0.69	0.69	-0.69	0.68
$H+O\rightarrow OH$	-1.61	1.61	-0.036	1.61
$H_2+O\rightarrow OH+H$	-0.46	0.46	-0.21	0.46
$HO_2+OH\rightarrow H_2O+O_2$	-1.14	1.15	-0.93	1.15
$H_2+OH\rightarrow H_2O+H$	-0.43	0.49	-0.43	0.42
$O_2+H\rightarrow OH+O$	-0.22	0.23	-0.11	0.23

Two-dimensional projections of F on pairs of x's reveal their mutual correlation. Examples of possible outcomes are shown in Figure 7. The top left panel in Figure 7 demonstrates the absence of correlation: any pair of values of the rate coefficients of reactions HCO + O → CO + OH and HCCO + O_2 → CO_2 + CO + H within their respective [x_{min} x_{max}] bounds is feasible. The top right panel also shows a case of no correlation, but now while any of the [x_{min} x_{max}] values for reaction CH + O → CO + H is feasible, for reaction CO + OH → CO_2 + H only values within a narrower range, about [$10^{-0.15}$, $10^{-0.2}$] are feasible. The bottom left panel shows a positive correlation, with higher values of x(O_2 + H → OH + O) feasible only with higher values of x(O_2 + H → HO_2) and vice versa, and the bottom right panel shows a negative correlation and it is substantially shifted from the initial recommendations, represented by the central point, [0 0]. A collection of all two-dimensional projections informs on the structure of the feasible set, F. One can also explore three- or four-dimensional correlation plots.

Projections of F on parameter-QoI pairs depict correlations of the parameter and QoI uncertainties. Several such examples are presented in Figure 8. Furthermore, the B2B-DC framework also allows one to examine correlations among QoI uncertainties. These examples are shown in Figure 9. It is pertinent to note that the initially selected QoI were assumed uncorrelated. The correlations exposed in Figure 9 have their origin in the constraints imposed in the model-data system, the DLR-SynG 2 dataset. For instance, the bottom-left panel of Figure 9 indicates that predictions for the flame speed of QoI a00000535 and ignition delay time of QoI a00000318 can have only values represented by the blue region. The latter originates from the kinetic model being constrained to reproduce the rest of the experimental observations within their respective ranges of uncertainties.

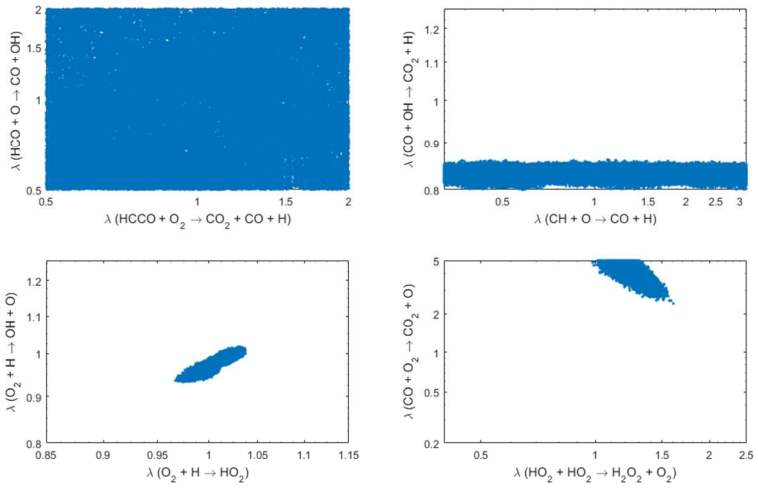

Figure 7. Two-dimensional projections of feasible set F on pairs of x's; the axes are logarithms of rate coefficient multipliers of the indicated reactions, λ. Their ranges represent the uncertainty bounds.

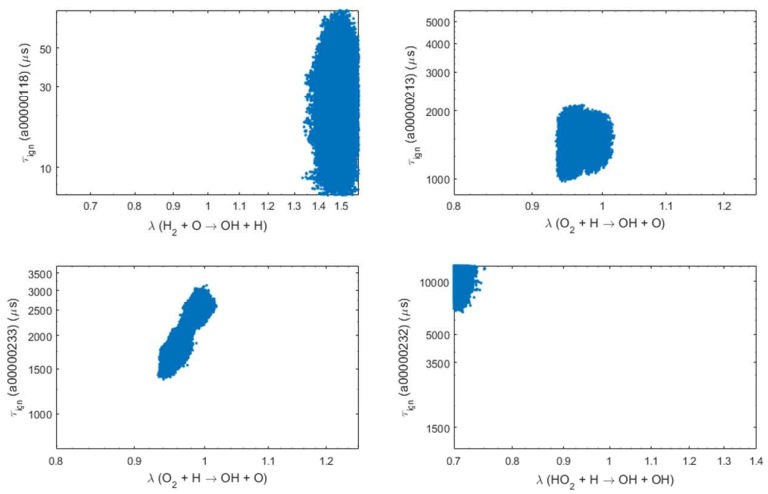

Figure 8. Two-dimensional projections of feasible set F on parameter-QoI pairs; the horizontal axes are rate-coefficient multipliers, λ, of the indicated reactions, the vertical axes are QoI values. The axes ranges represent the uncertainty bounds.

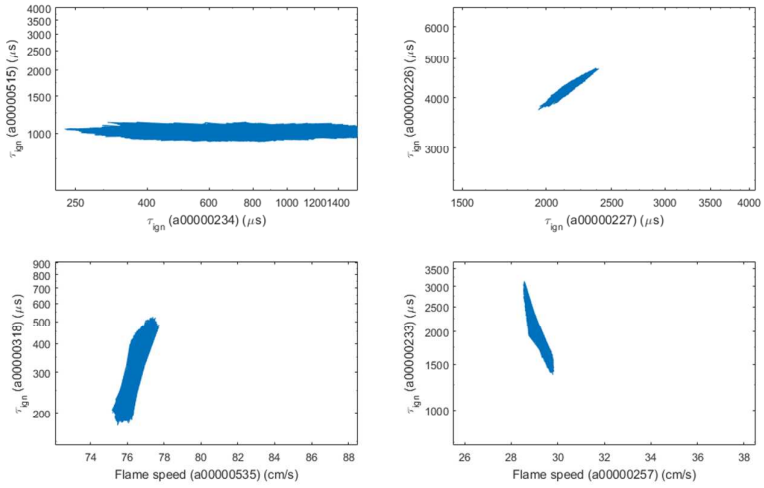

Figure 9. Two-dimensional projections of feasible set F on QoI pairs. The axes are QoI values; their ranges represent the uncertainty bounds.

5.3. Parameter Optimization. While the primary focus of the B2B-DC framework is on prediction over the feasible set, it also supports parameter optimization.[120] Four sets of optimized model parameters were investigated and inter-compared in the present study. The first approach is LS-H, a (weighted) least-squared fit constraining parameter values to their initially assessed uncertainty ranges, H. This is now a common approach.[2,10,24,27,114,117,118] B2B-DC supports two more refined methods of optimization,[120] LS-F and 1N-F, where the objective is minimized with x's being constrained to the feasible set F. The three problems are easily expressed as mathematical optimizations. The LS methods minimize the familiar sum of weighted least-squared deviations between the surrogate model prediction and the reported measured value, y_e. The difference lies in where the search takes place: LS-H considers all of H while LS-F restricts the search to F,

$$\text{LS-H}: \quad \min_{x\in \text{H}} \sum_e w_e \left[M_e(x) - y_e \right]^2$$

$$\text{LS-F}: \quad \min_{x\in \text{F}} \sum_e w_e \left[M_e(x) - y_e \right]^2$$

By contrast, the 1N-F problem treats the nominal parameter vector, the starting set of parameter values ($x_0 = 0$), as "preferred". As we saw it in Section 5.1, this parameter set lies outside the feasible region F. The goal of the 1N-F method is to find with fewest number of changes to x_0 a parameter vector that is feasible. Mathematically, the one-norm, $\|\cdot\|_1$, is a well-known approximation to enforce such sparsity,[171] i.e.,

$$\text{1N-F}: \quad \min_{x\in \text{F}} \|x - x_0\|_1$$

The LS-F and 1N-F optimizations were performed with the final dataset, DLR-SynG 2, as the two methods are designed to work with an existing feasible set. Finally, the fourth set of parameters we examined is the one corresponding to the single consistent point of the DLR-SynG 1 dataset, resulted from the VCM optimization.[169]

The average deviations of the optimized-model predictions from the experimental observations are depicted in Figure 10; the deviations for all individual experiments are given in Figure S1 of the Supporting Information. Some of the individual comparisons are shown in Figures 11-18, with the inclusion of the most recent literature model.[116] Experimental targets of the DLR-SynG dataset in these figures are designated by a star, the 8 self-inconsistent QoI (excluded from the DLR-SynG 0, Table 4) are colored red and those excluded from DLR-SynG 1 (listed in Tables 5 and 6) are colored green.

Inspection of the results displayed in Figure 10 highlights several features. All optimization methods result in parameter sets that produce a better agreement with experiment than the original set, composed of literature recommendations. The LS-H optimization, constrained only to the prior uncertainty ranges of parameters, results in the lowest average deviation, as expected, but at the expense of violating uncertainty bounds of 13 experimental QoI. Only the LS-F and 1N-F optimization methods, with additional constraints to the QoI uncertainties, do not violate any of the QoI bounds, by design. The average deviation produced by LS-F is larger but not significantly than that of LS-H. The 1N-F method gives a larger average deviation, yet it changes the least number of variables, as shown in Figure S2 of Supporting Information.

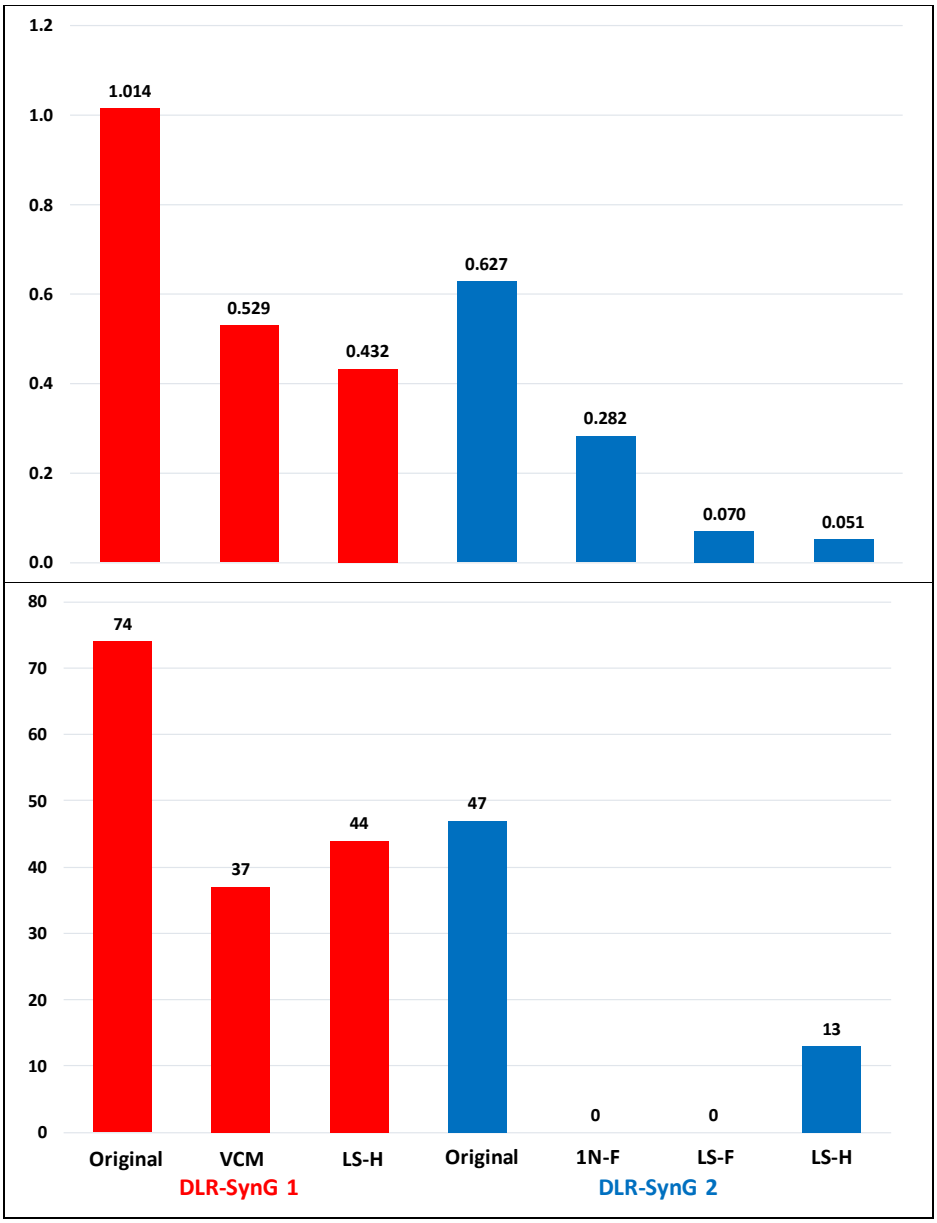

Figure 10. Top: average sum-of-squares deviations of the optimized-model predictions from the experimental observations. Bottom: number of bound violations, i.e., when model-predicted QoI values are outside their respective uncertainty bounds. The individual bars correspond to the indicated parameter sets: "Original" represents the initial literature-value set (Table S5 of Supporting Information) and the rest designate the optimization methods of the present work. Colored in red are results obtained with the DLR-SynG-1 dataset and colored in blue are those obtained with the DLR-SynG-2 dataset.

An explicit comparison is shown for some of the QoI in Figures 11-17, as well as in Figures S3-S7 of Supporting Information. The visual observation is that all the optimized models seem to perform with about the same overall quality: some models do better for one set of conditions, while other are closer to other experimental data sets (see Figures 11-13, 17, S3-S5). The shock-tube ignition delay times show a larger variation between different models. The problem here could lie with the incomplete instrumental model[172] used in the simulation of ignition phenomena, as it does not capture the "non-idealities" of shock-tube experiments with sufficient detail,[127] or the development of a mild-ignition regime,[130] which is not entirely driven by chemistry. These factors are especially under suspicion in the inconsistent ignition-delay targets. Generally, the laminar flame speeds are

predicted better by all models, with all simulations falling within the uncertainties bounds of experimental observations (see Figures 14-17, S6-S7), reflecting perhaps the higher experimental accuracy of the measurements.[173]

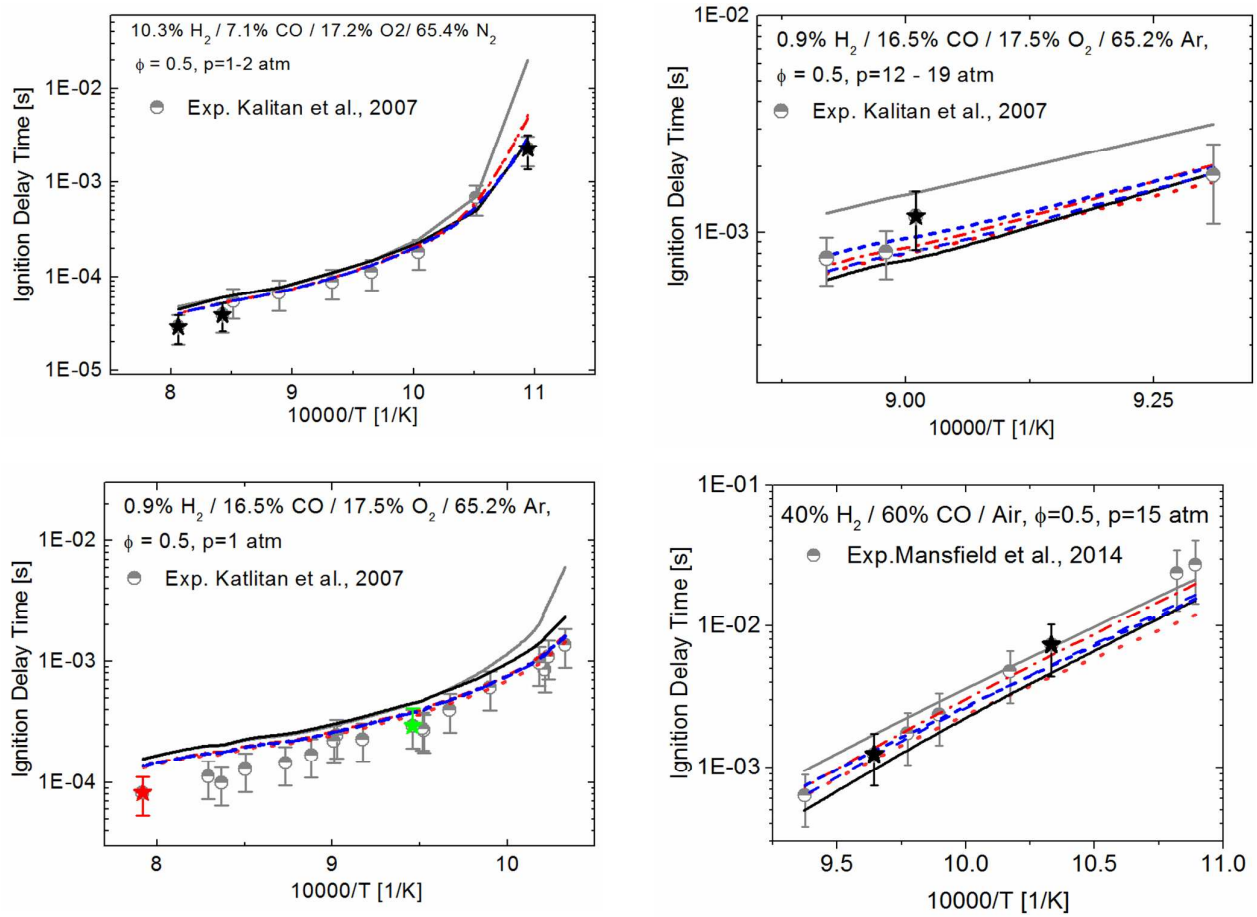

Figure 11. Ignition delay times: symbols, experimental data;[67,103] initial model, black line; Varga et al.[116] model, gray line; LS-H, red dotted line; VCM, red dash-dotted line; LS-F, blue dashed line; 1N-F, blue short-dash line. Black stars are targets of DLR-SynG 2 dataset; red stars are self-inconsistent targets; green stars are targets deleted from DLR-SynG 1 dataset.

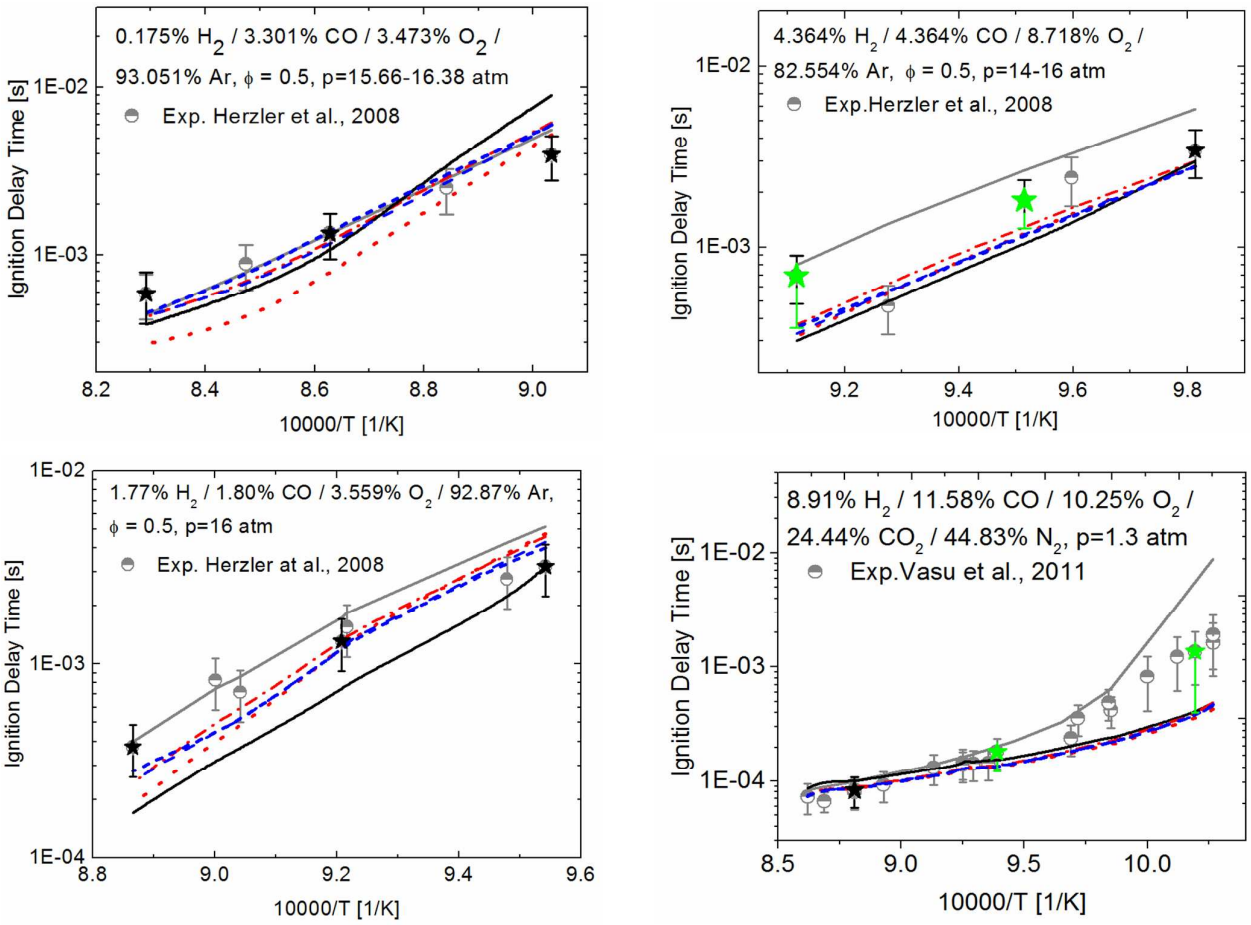

Figure 12. Ignition delay times: symbols, experimental data;[86,106] initial model, black line; Varga et al.[116] model, gray line; LS-H, red dotted line; VCM, red dash-dotted line; LS-F, blue dashed line; 1N-F, blue short-dash line. Black stars are targets of DLR-SynG 2 dataset; green stars are targets deleted from DLR-SynG 1 dataset.

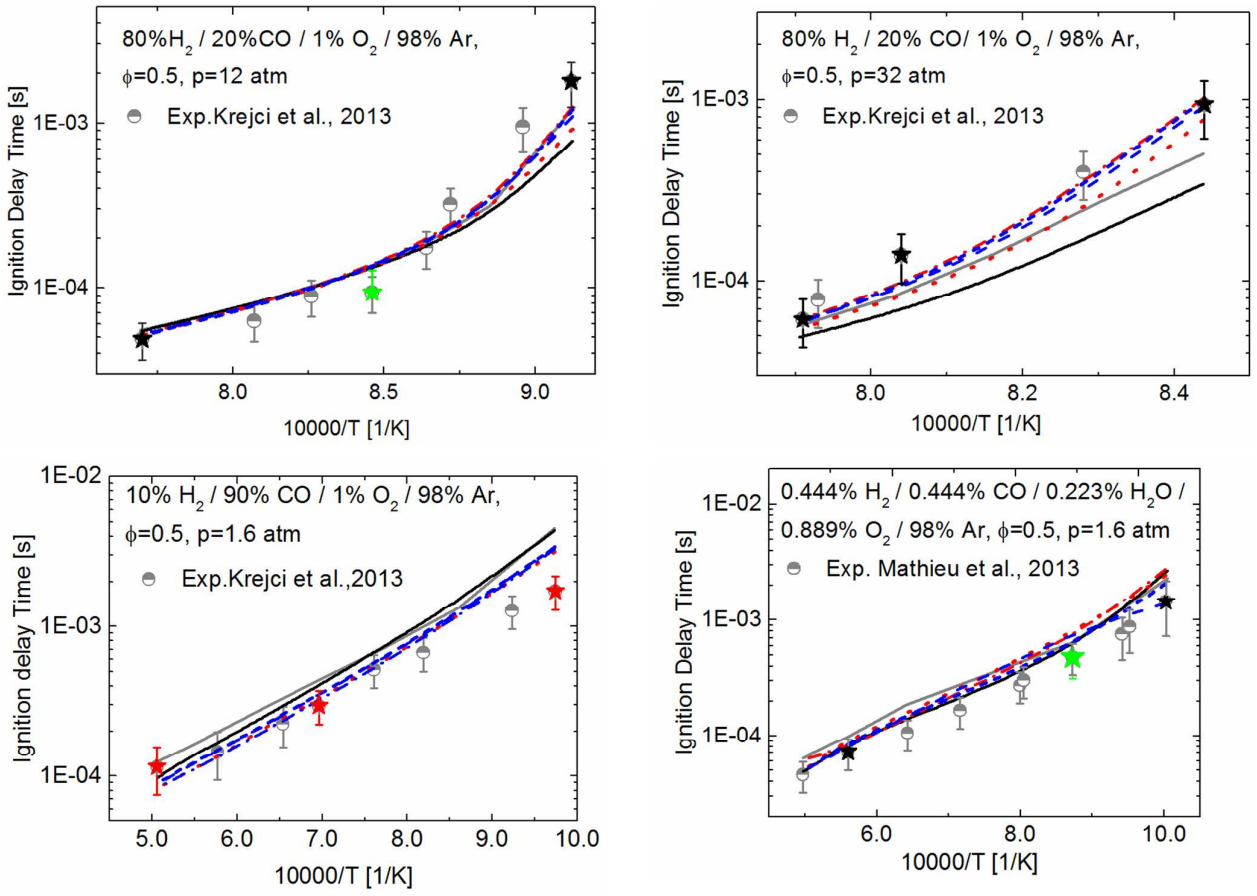

Figure 13. Laminar flame speeds: symbols, experimental data;[73,104] initial model, black line; Varga et al.[116] model, gray line; LS-H, red dotted line; VCM, red dash-dotted line; LS-F, blue dash line; 1N-F, blue short dash line. Black stars are targets of DLR-SynG 2 dataset; green stars are targets deleted from DLR-SynG 1 dataset.

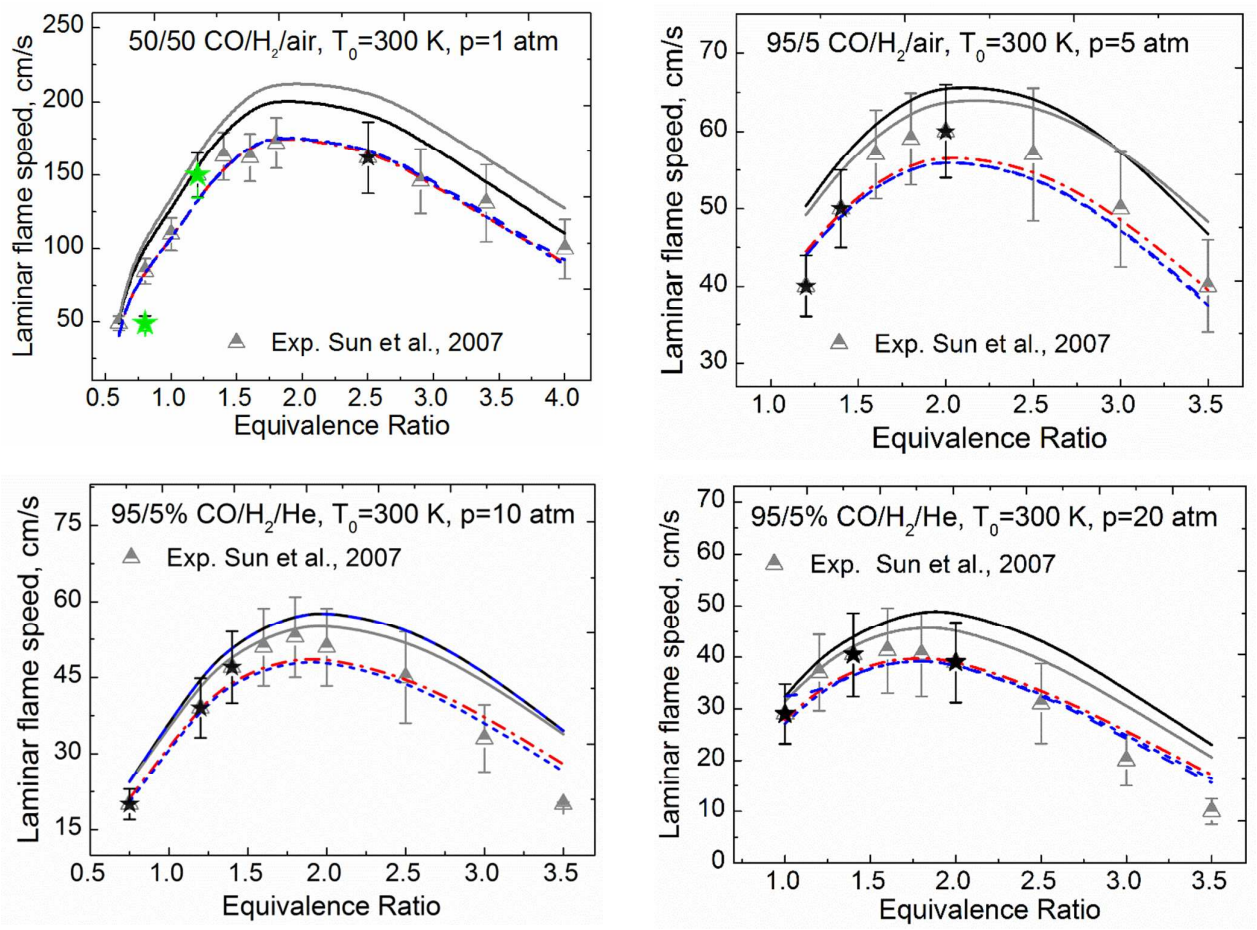

Figure 14. Laminar flame speeds: symbols, experimental data;[20] initial model, black line; Varga et al.[116] model, gray line; LS-H, red dotted line; VCM, red dash-dotted line; LS-F, blue dash line; 1N-F, blue short dash line. Black stars are targets of DLR-SynG 2 dataset; green stars are targets deleted from DLR-SynG 1 dataset.

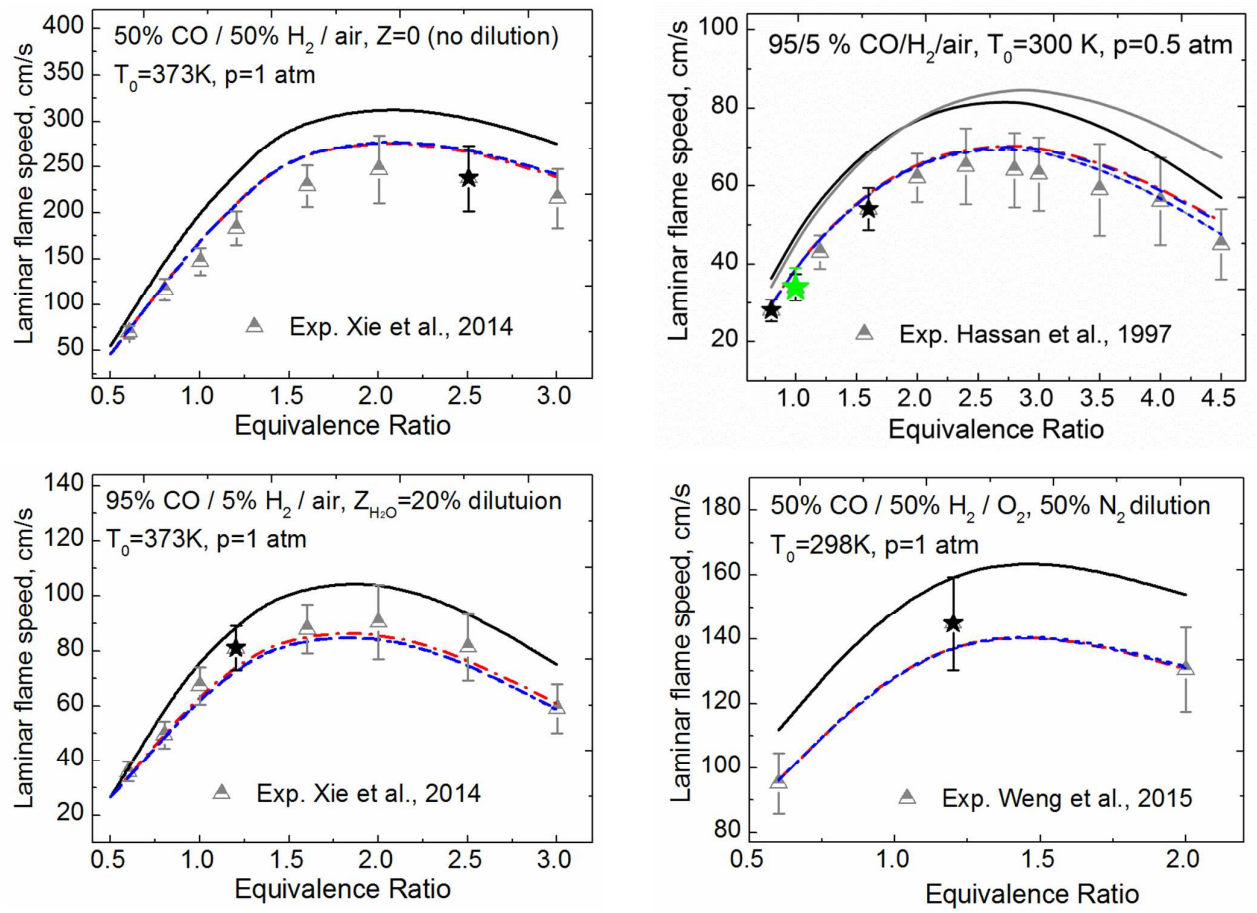

Figure 15. Laminar flame speeds: symbols, experimental data;[51,81,97] initial model, black line; Varga et al.[116] model, gray line; LS-H, red dotted line; VCM, red dash-dotted line; LS-F, blue dash line; 1N-F, blue short dash line. Black stars are targets of DLR-SynG 2 dataset; green stars are targets deleted from DLR-SynG 1 dataset.

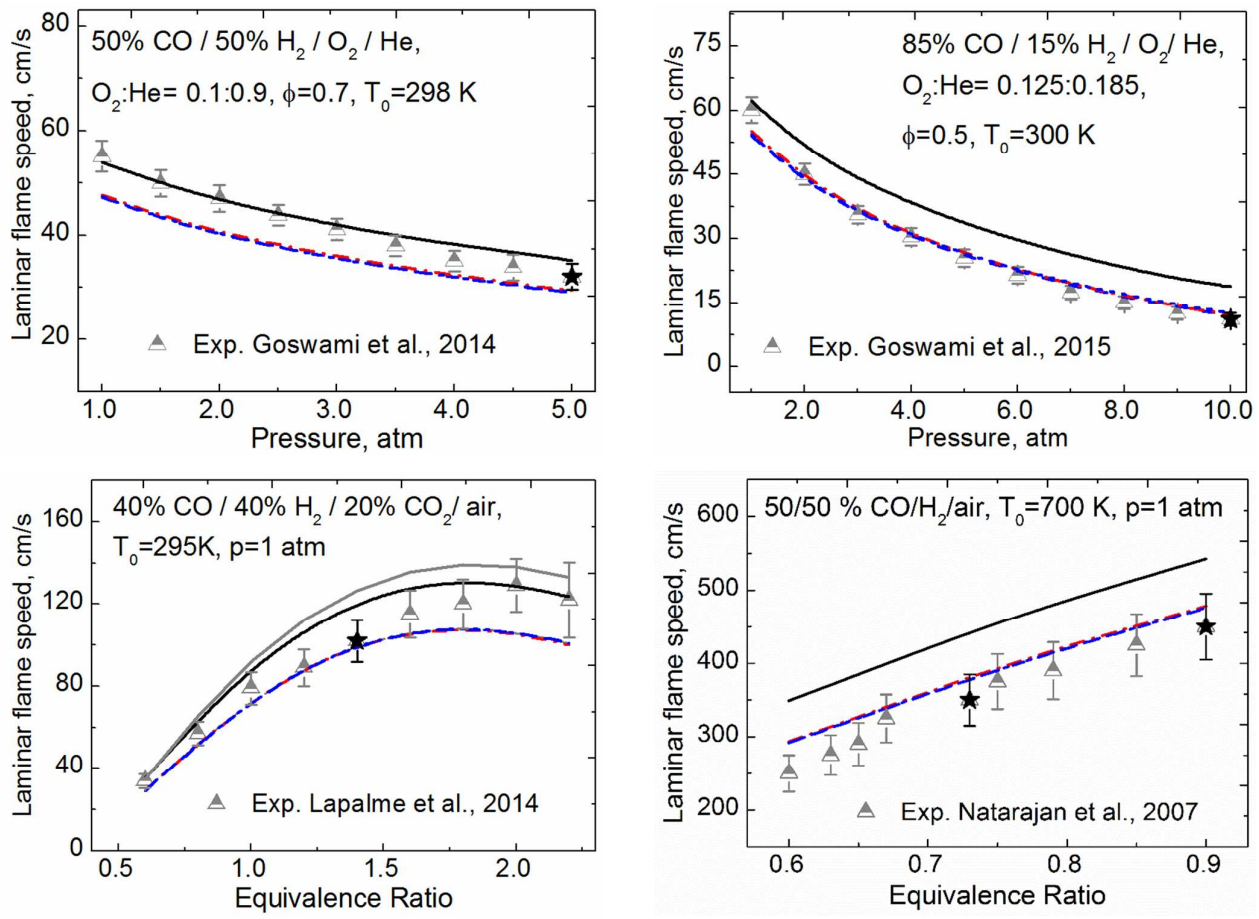

Figure 16. Laminar flame speeds: symbols, experimental data;[25,75,80,107] initial model, black line; Varga et al.[116] model, gray line; LS-H, red dotted line; VCM, red dash-dotted line; LS-F, blue dash line; 1N-F, blue short dash line. Black stars are targets of DLR-SynG 2 dataset.

5.4. Model Prediction. As was mentioned earlier, one of the key features of the B2B-DC methodology is prediction on the feasible set. The existence of the feasible set is established by forming a dataset and examining its consistency, the procedure that can be referred to as *model validation*. Once the feasible set is established and the model is validated, one can examine a model's prediction for a QoI that was *not* included in the validating dataset, referred to as a blind prediction.

First, we made blind predictions for experimentally observed QoI that were not included in the dataset. The results are reported in Figure 17; they include three sets of ignition delay times and one set of laminar flame speeds. The two sets of ignition delays, displayed in the left two panels of Figure 17, are those measured in highly dilute mixtures. In these cases, the predictions of all the models are grouped closely together. On the other hand, the predictions for the other two cases, ignition delays (top right) and laminar flame speeds (bottom right) for non-dilute mixtures, show significant differences. The predictions of B2B-DC-optimized models are all grouped together and are essentially within the reported uncertainties of the experimental observations. The initial model predicts the ignition delay times within their uncertainties and the laminar flame speeds reasonably close to their upper uncertainty bounds. The model of Varga et al.[116] substantially overshoots the upper uncertainty bounds in both cases.

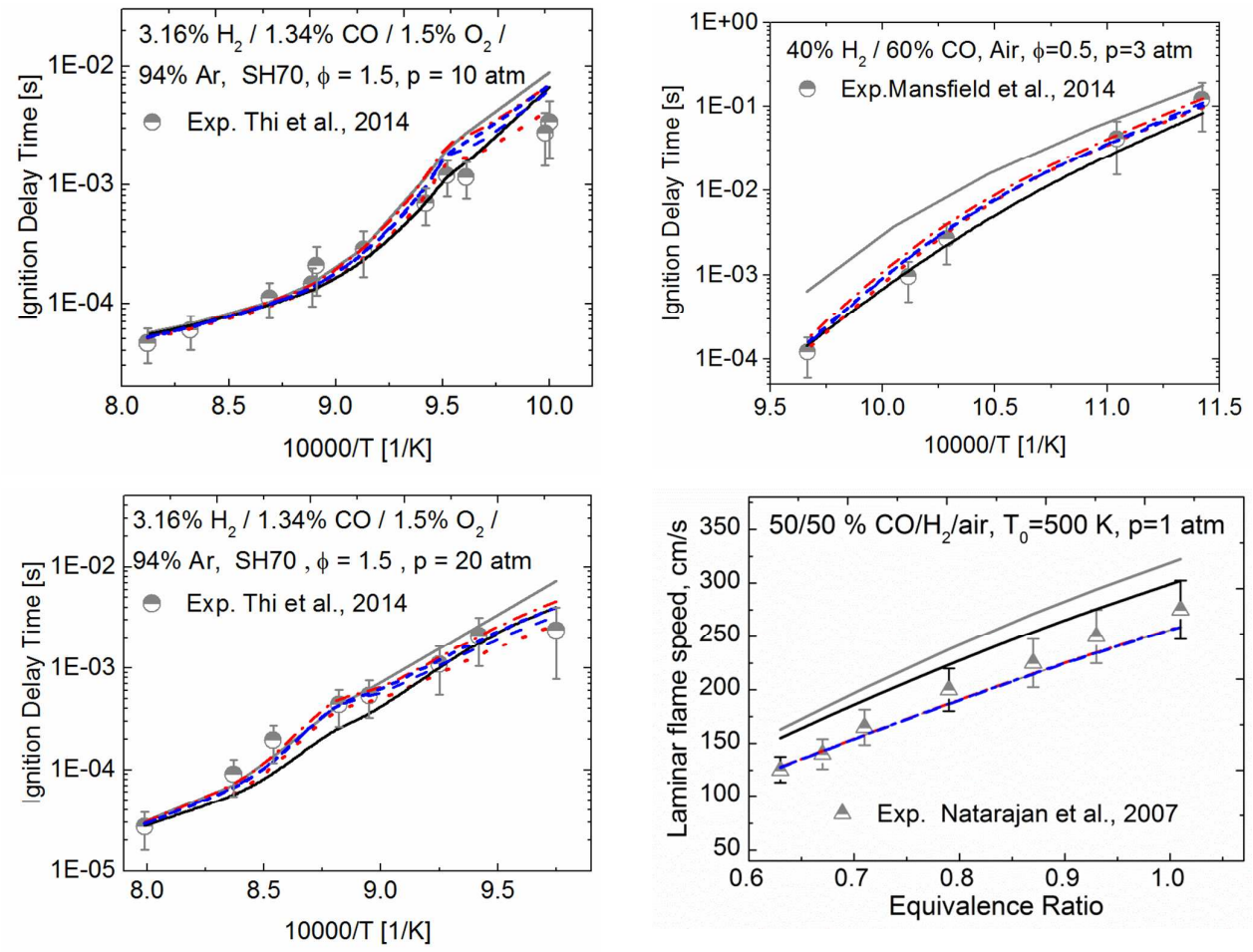

Figure 17. Ignition delay times[74,103] and laminar flame speeds:[75] symbols, experimental data; initial model, black line; Varga et al.[116] model, gray line; LS-H, red dotted line; VCM, red dash-dotted line; LS-F, blue dash line; 1N-F, blue short dash line.

In the next test of blind prediction, we focused on what one may consider extreme operating conditions of a combustor, having a fuel with a low heating value at low temperatures and high pressures. Specifically, we selected a fuel mixture containing 1.0 % H_2, 5.3 % CO, 42.7 % H_2O, and 51.1 % CO_2 that is mixed with pre-heated air under fuel-lean conditions, $\phi = 0.5$, $p = 12$ bar, and $T = 720$-820 K.

The model predictions are displayed in Figure 15, along with those of Varga et al.[116] Also shown, as black vertical lines, are uncertainty intervals computed using B2B-DC with the DLR-SynG 2 dataset. These intervals reflect all the uncertainty information of the DLR-SynG 2 dataset, those of the parameters and those of the dataset targets. Inspection of the results depicted in Figure 15 indicates that all models but one, LS-H, predict the new target within the B2B-DC-predicted bounds. The LS-H predictions are definitely outside the bounds. This outcome is not unexpected, as is suggested by our Conclusions.

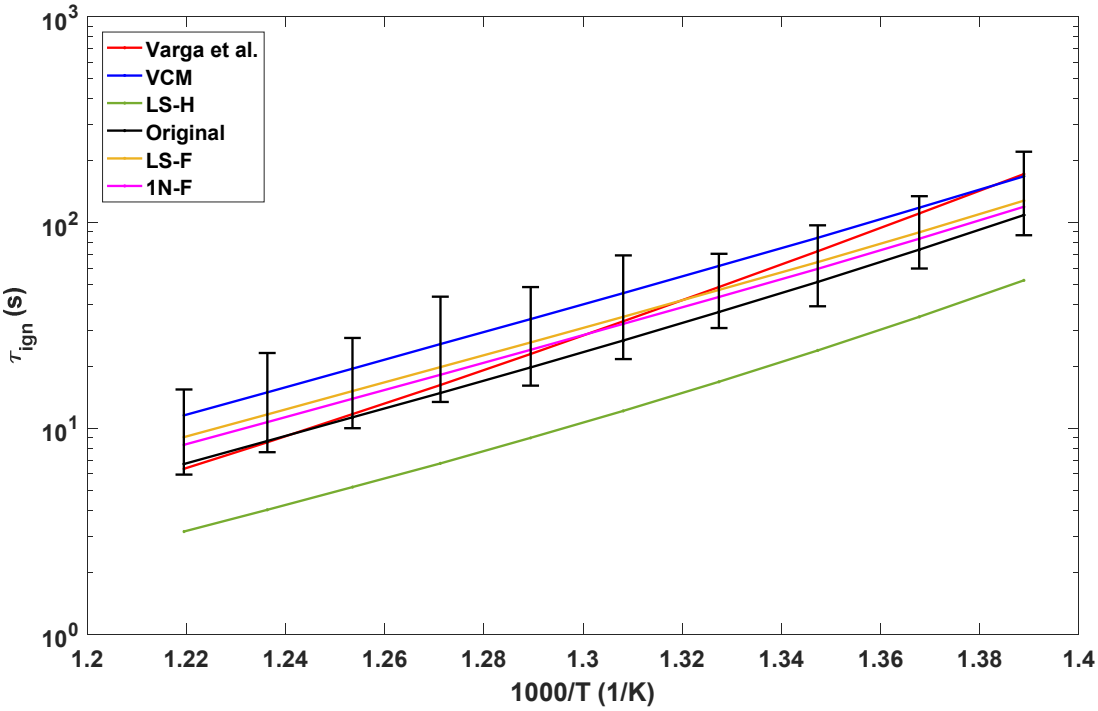

Figure 15. Ignition delay times: initial model, black solid line; Varga et al.[116] model, red; LS-H, green; VCM, blue; LS-F, yellow; 1N-F, purple; uncertainty intervals, black vertical bars.

6. CONCLUSIONS

Developing *predictive* models[2] has become the goal in much of the modeling studies of reaction systems. Numerical optimization of complex reaction networks, of the kind that guided the development of GRI-Mech,[2,10,114] has now been accepted as one of the underlying methods in this pursuit (see, e.g., recent publications[24,27,117]). In the language of the present work, this is the LS-H approach, a least-squares minimization constrained to a priori selected parameter ranges. The results of the present study, however, demonstrate that the LS-H optimization may miss some critical information of the model-data system.

It has been known for some time (see Frenklach[174] and references cited therein) that it is rather unproductive to search for a single optimal point in analysis of chemical kinetics, as the nature of the problem leads to correlated regions in parameter space, having many (if not infinite number) of such optimal points with practically indistinguishable predictions. The present results further demonstrate such outcomes.

Whether it is statistically established confidence region[174] (or credible region in the present Bayesian terminology) or deterministically defined feasible set,[6,11] analysis based on these regions of "optimality" should be more informative. Indeed, as we saw with the present results, the LS-H minimization produces the lowest-value deviation, and yet there are a substantial number of individual predictions that exceed the prescribed experimental uncertainty. The practical implication of such an outcome can be paraphrased as follows: the LS-H optimization hides the truth by averaging good with bad.

On the other hand, the consistency analysis of B2B-DC, probing the feasible-set existence, immediately identified inconsistent experimental targets. This mathematical result does not identify whether the problem is with the model itself, its parameter values, or experimental observations—these are the questions for the combustion and kinetics scientists to resolve—but it does identify where to look.

For the particular system we analyzed, the suspicion is on the instrumental models used to simulate the ignition. The future will tell if our present speculation on the possible source of the inconsistency is correct or not. What is definite, however, is that the feasible-set analysis of B2B-DC identified the problem otherwise hidden in "averaged" least-squares optimization.

ASSOCIATED CONTENT

Supporting Information

List of tables

Table S1. Ignition delay time measurements
Table S2. Laminar flame speed measurements from Experimental Data for PrIMe Flame Speed
Table S3. Ignition delay QoI
Table S4. Laminar flame speed QoI
Table S5. Input reaction model
Table S6. Active variables, λ

List of figures

Figure S1. Relative deviations of the optimized-model predictions from the experimental observations, corresponding to the cases depicted in Figure 10 of the manuscript.
Figure S2. Change in model parameters as a result of optimization with the DLR-SynG-2 dataset using LS-H and 1N-F methods.
Figures S3-S5. Comparison of computed and experimental ignition delay times.
Figures S6-S7. Comparison of computed and experimental laminar flame speeds.

AUTHOR INFORMATION

Corresponding Authors

(N. A. Slavinskaya) E-mail: nadja.slavinskaya@dlr.de
(M. Frenklach) E-mail: frenklach@berkeley.edu

Notes

The authors declare no competing financial interest.

ACKNOWLEDGMENTS

The UCB authors acknowledge the support of the U. S. Department of Energy, National Nuclear Security Administration, under award DE-NA0002375. The views and opinions of authors expressed herein do not necessarily state or reflect those of the United States Government or any agency thereof.

References

(1) Frenklach, M. PrIMe. http://primekinetics.org.
(2) Frenklach, M. *Proc. Combust. Inst.*, **2007**, *31*, 125–140.
(3) You, X.; Packard, A.; Frenklach, M. *Int. J. Chem. Kinet.*, **2012**, *44*, 101–116.

(4) Slavinskaya, N. A.; Frank, P. *Combust. Flame*, **2009**, *156*, 1705–1722.
(5) Slavinskaya, N. A.; Riedel, U.; Dworkin, S. B.; Thomson, M. J. *Combust. Flame*, **2012**, *159*, 979–995.
(6) Frenklach, M.; Packard, A.; Seiler, P.; Feeley, R. *Int. J. Chem. Kinet.*, **2004**, *36*, 57–66.
(7) Feeley, R.; Seiler, P.; Packard, A.; Frenklach, M. *J. Phys. Chem. A*, **2004**, *108*, 9573–9583.
(8) Russi, T.; Packard, A.; Feeley, R.; Frenklach, M. *J. Phys. Chem. A*, **2008**, *112*, 2579–2588.
(9) Russi, T.; Packard, A.; Frenklach, M. *Chem. Phys. Lett.*, **2010**, *499*, 1–8.
(10) Frenklach, M.; Packard, A.; Feeley, R. in *Modeling of Chemical Reactions (R. W. Carr, Ed.)*, Compr. Chem. Kinet. v. 42; Elsevier: Amsterdam, London, New York, 2007, pp. 243–291.
(11) Seiler, P.; Frenklach, M.; Packard, A.; Feeley, R. *Optim. Eng.*, **2006**, *7*, 459–478.
(12) Baulch, D. L. *J. Phys. Chem. Ref. Data*, **2005**, *34*, 757.
(13) Zsély, I. G.; Zádor, J.; Turányi, T. *Proc. Combust. Inst.*, **2005**, *30*, 1273–1281.
(14) Yetter, R. A.; Dryer, F. L.; Rabitz, H. *Combust. Sci. Technol.*, **1991**, *79*, 97–128.
(15) Davis, S. G.; Joshi, A. V.; Wang, H.; Egolfopoulos, F. *Proc. Combust. Inst.*, **2005**, *30*, 1283–1292.
(16) Saxena, P.; Williams, F. A. *Combust. Flame*, **2006**, *145*, 316–323.
(17) Petrova, M.; Williams, F. *Combust. Flame*, **2006**, *144*, 526–544.
(18) Li, J.; Zhao, Z.; Kazakov, A.; Chaos, M.; Dryer, F. L.; Scire, J. J. *Int. J. Chem. Kinet.*, **2007**, *39*, 109–136.
(19) Chaos, M.; Dryer, F. L. *Combust. Sci. Technol.*, **2008**, *180*, 1053–1096.
(20) Sun, H.; Yang, S. I.; Jomaas, G.; Law, C. K. *Proc. Combust. Inst.*, **2007**, *31*, 439–446.
(21) Frassoldati, A.; Faravelli, T.; Ranzi, E. *Int. J. Hydrogen Energy*, **2007**, *32*, 3471–3485.
(22) Le Cong, T.; Dagaut, P.; Dayma, G. *J. Eng. Gas Turbines Power*, **2008**, *130*, 041502.
(23) Cavaliere, D. E.; Joannon, M. d.; Sabia, P.; Sirignano, M.; D'Anna, A. *Combust. Sci. Technol.*, **2010**, *182*, 692–701.
(24) Kéromnès, A.; Metcalfe, W. K.; Heufer, K. A.; Donohoe, N.; Das, A. K.; Sung, C.-J.; Herzler, J.; Naumann, C.; Griebel, P.; Mathieu, O.; Krejci, M. C.; Petersen, E. L.; Pitz, W. J.; Curran, H. J. *Combust. Flame*, **2013**, *160*, 995–1011.
(25) Goswami, M.; Bastiaans, R.; Konnov, A. A.; Goey, L. de. *Int. J. Hydrogen Energy*, **2014**, *39*, 1485–1498.
(26) Nilsson, E. J. K.; Konnov, A. A. *Energy Fuels*, **2016**, *30*, 2443–2457.
(27) Varga, T.; Olm, C.; Nagy, T.; Zsély, I. G.; Valkó, É.; Pálvölgyi, R.; Curran, H. J.; Turányi, T. *Int. J. Chem. Kinet.*, **2016**, *48*, 407–422.
(28) Ó Conaire, M.; Curran, H. J.; Simmie, J. M.; Pitz, W. J.; Westbrook, C. K. *Int. J. Chem. Kinet.*, **2004**, *36*, 603–622.
(29) Konnov, A. A. *Combust. Flame*, **2008**, *152*, 507–528.
(30) Konnov, A. A. *Combust. Flame*, **2009**, *156*, 2093–2105.
(31) Alekseev, V. A.; Christensen, M.; Konnov, A. A. *Combust. Flame*, **2015**, *162*, 1884–1898.
(32) Starik, A. M.; Titova, N. S.; Sharipov, A. S.; Kozlov, V. E. *Combust. Explos. Shock Waves*, **2010**, *46*, 491–506.
(33) Sun, S.; Meng, S.; Zhao, Y.; Xu, H.; Guo, Y.; Qin, Y. *Int. J. Hydrogen Energy*, **2016**, *41*, 3272–3283.
(34) Dean, A. M.; Steiner, D. C.; Wang, E. E. *Combust. Flame*, **1978**, *32*, 73–83.
(35) Yetter, R. A.; Dryer, F. L.; Rabitz, H. *Combust. Sci. Technol.*, **1991**, *79*, 129–140.
(36) Arustamyan, A. M.; Shakhnazaryan, I. K.; Philipossyan, A. G.; Nalbandyan, A. B. *Int. J. Chem. Kinet.*, **1980**, *12*, 55–75.
(37) Gardiner, W. C.; McFarland, M.; Morinaga, K.; Takeyama, T.; Walker, B. F. *J. Phys. Chem.*, **1971**, *75*, 1504–1509.
(38) Egolfopoulos, F. N.; Law, C. K. *Proc. Combust. Inst.*, **1991**, *23*, 333–340.
(39) Vagelopoulos, C. M.; Egolfopoulos, F. N.; Law, C. K. *Proc. Combust. Inst.*, **1994**, *25*, 1341–1347.
(40) Dowdy, D. R.; Smith, D. B.; Taylor, S. C.; Williams, A. *Proc. Combust. Inst.*, **1991**, *23*, 325–332.
(41) Aung, K. T.; Hassan, M. I.; Faeth, G. M. *Combust. Flame*, **1997**, *109*, 1–24.
(42) Aung, K. T.; Hassan, M. I.; Faeth, G. M. *Combust. Flame*, **1998**, *112*, 1–15.
(43) Kwon, O.; Faeth, G. *Combust. Flame*, **2001**, *124*, 590–610.
(44) Karpov, V. P.; Lipatnikov, A. N.; Wolanski, P. *Combust. Flame*, **1997**, *109*, 436–448.

(45) McLean, I. C.; Smith, D. B.; Taylor, S. C. *Proc. Combust. Inst.*, **1994**, *25*, 749–757.
(46) Vagelopoulos, C. M.; Egolfopoulos, F. N. *Proc. Combust. Inst.*, **1994**, *25*, 1317–1323.
(47) Kim, T. J.; Yetter, R. A.; Dryer, F. L. *Proc. Combust. Inst.*, **1994**, *25*, 759–766.
(48) Lewis, B.; Elbe, G. von. *Combustion, Flames, and Explosions of Gases*, 3rd ed.; Academic Press: Orlando, 1987.
(49) Huang, Y.; Sung, C.; Eng, J. *Combust. Flame*, **2004**, *139*, 239–251.
(50) Mueller, M. A.; Yetter, R. A.; Dryer, F. L. *Int. J. Chem. Kinet.*, **1999**, *31*, 705–724.
(51) Mittal, G.; Sung, C.-J.; Yetter, R. A. *Int. J. Chem. Kinet.*, **2006**, *38*, 516–529.
(52) Sivaramakrishnan, R.; Comandini, A.; Tranter, R. S.; Brezinsky, K.; Davis, S. G.; Wang, H. *Proc. Combust. Inst.*, **2007**, *31*, 429–437.
(53) Fotache, C. G.; Tan, Y.; Sung, C. J.; Law, C. K. *Combust. Flame*, **2000**, *120*, 417–426.
(54) Kalitan, D. M.; Petersen, E. L. AIAA Paper No. 2005-3767. *41st AIAA/ASME/SAE/ASEE Joint Propulsion Conference and Exhibit.* Tucson, AZ, 2005.
(55) Xia, Y. PhD Thesis, Aberystwyth, Wales, 2000.
(56) Scholte, T. G.; Vaags, P. B. *Combust. Flame*, **1959**, *3*, 511–524.
(57) Hassan, M. I.; Aung, K. T.; Faeth, G. M. *J. Propul. Power*, **1997**, *13*, 239–245.
(58) Konnov, A. A.; Dyakov, I. V.; Ruyck, J. de. *Proc. Combust. Inst.*, **2002**, *29*, 2171–2177.
(59) Lewis, B.; Elbe, G. von. *Combustion, Flames, and Explosions of Gases*, 2rd ed.; Academic Press: Orlando, 1961.
(60) Dagaut, P.; Lecomte, F.; Mieritz, J.; Glarborg, P. *Int. J. Chem. Kinet.*, **2003**, *35*, 564–575.
(61) Alzueta, M. U.; Bilbao, R.; Glarborg, P. *Combust. Flame*, **2001**, *127*, 2234–2251.
(62) Glarborg, P.; Kubel, D.; Dam-Johansen, K.; Chiang, H.-M.; Bozzelli, J. W. *Int. J. Chem. Kinet.*, **1996**, *28*, 773–790.
(63) Vandooren, J.; van Tiggelen, P. J.; Pauwels, J.-F. *Combust. Flame*, **1997**, *109*, 647–668.
(64) Burke, M. P.; Qin, X.; Ju, Y.; Dryer, F. L. Paper No. A16. *5th Us Combustion Meeting.* San Diego, CA, 2007.
(65) Natarajan, J.; Kochar, Y.; Lieuwen, T.; Seitzman, J. *Proc. Combust. Inst.*, **2009**, *32*, 1261–1268.
(66) Dagaut, P. *Fuel*, **2003**, *82*, 1033–1040.
(67) Kalitan, D. M.; Mertens, J. D.; Crofton, M. W.; Petersen, E. L. *J. Propul. Power*, **2007**, *23*, 1291–1301.
(68) Petersen, E. L.; Kalitan, D. M.; Barrett, A. B.; Reehal, S. C.; Mertens, J. D.; Beerer, D. J.; Hack, R. L.; McDonell, V. G. *Combust. Flame*, **2007**, *149*, 244–247.
(69) Peschke, W. T.; Spadaccini, L. J. *Determination of autoignition and flame speed characteristics of coal gases having medium heating values*. Report EPRI AP-4291; East Hartford, Connecticut, 1985.
(70) Prathap, C.; Ray, A.; Ravi, M. R. *Combust. Flame*, **2008**, *155*, 145–160.
(71) Dong, C.; Zhou, Q.; Zhao, Q.; Zhang, Y.; Xu, T.; Hui, S. *Fuel*, **2009**, *88*, 1858–1863.
(72) Bouvet, N.; Chauveau, C.; Gökalp, I.; Halter, F. *Proc. Combust. Inst.*, **2011**, *33*, 913–920.
(73) Krejci, M. C.; Mathieu, O.; Vissotski, A. J.; Ravi, S.; Sikes, T. G.; Petersen, E. L.; Kérmonès, A.; Metcalfe, W.; Curran, H. J. *J. Eng. Gas Turbines Power*, **2013**, *135*, 021503.
(74) Thi, L. D.; Zhang, Y.; Huang, Z. *Int. J. Hydrogen Energy*, **2014**, *39*, 6034–6043.
(75) Natarajan, J.; Lieuwen, T.; Seitzman, J. *Combust. Flame*, **2007**, *151*, 104–119.
(76) Burbano, H. J.; Pareja, J.; Amell, A. A. *Int. J. Hydrogen Energy*, **2011**, *36*, 3232–3242.
(77) Ratna Kishore, V.; Ravi, M. R.; Ray, A. *Combust. Flame*, **2011**, *158*, 2149–2164.
(78) Singh, D.; Nishiie, T.; Tanvir, S.; Qiao, L. *Fuel*, **2012**, *94*, 448–456.
(79) Burke, M. P.; Chaos, M.; Dryer, F. L.; Ju, Y. *Combust. Flame*, **2010**, *157*, 618–631.
(80) Lapalme, D.; Seers, P. *Int. J. Hydrogen Energy*, **2014**, *39*, 3477–3486.
(81) Xie, Y.; Wang, J.; Xu, N.; Yu, S.; Huang, Z. *Int. J. Hydrogen Energy*, **2014**, *39*, 3450–3458.
(82) Li, X.; You, X.; Wu, F.; Law, C. K. *Proc. Combust. Inst.*, **2015**, *35*, 617–624.
(83) Abián, M.; Giménez-López, J.; Bilbao, R.; Alzueta, M. U. *Proc. Combust. Inst.*, **2011**, *33*, 317–323.
(84) Naumann, C.; Herzler, J.; Griebel, P.; Curran, H. J.; Kéromnès, A.; Mantzaras, I. *Results of ignition delay times for hydrogen-rich and syngas fuel mixtures measured*, 2011.
(85) Dean, A. M.; Johnson, R. L. *Combust. Flame*, **1980**, *37*, 109–123.

(86) Herzler, J.; Naumann, C. *Combust. Sci. Technol.*, **2008**, *180*, 2015–2028.
(87) Krejci, M. C.; Mathieu, O.; Vissotski, A. J.; Ravi, S.; Sikes, T. G.; Petersen, E. L.; Keromnes, A.; Metcalfe, W.; Curran, H. J. *ASME Turbo Expo 2012: Turbine Technical Conference and Exposition.* Copenhagen, Denmark, 2012.
(88) Thi, L. D.; Zhang, Y.; Fu, J.; Huang, Z.; Zhang, Y. *Can. J. Chem. Eng.*, **2014**, *92*, 861–870.
(89) Jahn, G. Der Zündvorgang in Gasgemischen, Oldenbourg, Berlin, 1934.
(90) Das, A. K.; Kumar, K.; Sung, C.-J. *Combust. Flame*, **2011**, *158*, 345–353.
(91) Bouvet, N.; Lee, S. Y.; Gökalp, I.; Santoro, R. *J. Proc. Europ. Combust. Meeting*, **2007**, *3*, 6–17.
(92) Zhang, X.; Huang, Z.; Zhang, Z.; Zheng, J.; Yu, W.; Jiang, D. *Int. J. Hydrogen Energy*, **2009**, *34*, 4862–4875.
(93) Kim, J. S.; Park, J.; Bae, D. S.; Vu, T. M.; Ha, J. S.; Kim, T. K. *Int. J. Hydrogen Energy*, **2010**, *35*, 1390–1400.
(94) Wu, F.; Kelley, A. P.; Tang, C.; Zhu, D.; Law, C. K. *Int. J. Hydrogen Energy*, **2011**, *36*, 13171–13180.
(95) Krejci, M. C.; Vissotski, A. J.; Ravi, S.; Metcalfe, W. K.; Kéromnès, A.; Curran, H. J.; Petersen, E. L. *Spring Technical Meeting of the Central States Section of the Combustion Institute.* Dayton, OH, 2012.
(96) Lohöfener, B.; Roungos, E.; Voss, S.; Trimis, D. *2nd Heat Flux Burner Workshop 2012*; Warsaw, Poland, 2012.
(97) Weng, W. B.; Wang, Z. H.; He, Y.; Whiddon, R.; Zhou, Y. J.; Li, Z. S.; Cen, K. F. *Int. J. Hydrogen Energy*, **2015**, *40*, 1203–1211.
(98) Voss, S.; Hartl, S.; Hasse, C. *Int. J. Hydrogen Energy*, **2014**, *39*, 19810–19817.
(99) Zhang, Y.; Shen, W.; Fan, M.; Zhang, H.; Li, S. *Combust. Flame*, **2014**, *161*, 2492–2495.
(100) Santner, J.; Dryer, F. L.; Ju, Y. *Proc. Combust. Inst.*, **2013**, *34*, 719–726.
(101) Linteris, G. T.; Yetter, R. A.; Brezinsky, K.; Dryer, F. L. *Combust. Flame*, **1991**, *86*, 162–170.
(102) Mertens, J. D.; Kalitan, D. M.; Barrett, A. B.; Petersen, E. L. *Proc. Combust. Inst.*, **2009**, *32*, 295–303.
(103) Mansfield, A. B.; Wooldridge, M. S. *Combust. Flame*, **2014**, *161*, 2242–2251.
(104) Mathieu, O.; Kopp, M. M.; Petersen, E. L. *Proc. Combust. Inst.*, **2013**, *34*, 3211–3218.
(105) Gersen, S.; Darmeveil, H.; Levinsky, H. *Combust. Flame*, **2012**, *159*, 3472–3475.
(106) Vasu, S. S.; Davidson, D. F.; Hanson, R. K. *Energy Fuels*, **2011**, *25*, 990–997.
(107) Goswami, M.; van Griensven, J.; Bastiaans, R.; Konnov, A. A.; Goey, L. de. *Proc. Combust. Inst.*, **2015**, *35*, 655–662.
(108) Han, M.; Ai, Y.; Chen, Z.; Kong, W. *Fuel*, **2015**, *148*, 32–38.
(109) He, Y.; Wang, Z.; Weng, W.; Zhu, Y.; Zhou, J.; Cen, K. *Int. J. Hydrogen Energy*, **2014**, *39*, 9534–9544.
(110) Li, H.-M.; Li, G.-X.; Sun, Z.-Y.; Zhou, Z.-H.; Li, Y.; Yuan, Y. *Exp. Therm. Fluid Sci.*, **2016**, *74*, 160–168.
(111) Wang, Z. H.; Weng, W. B.; He, Y.; Li, Z. S.; Cen, K. F. *Fuel*, **2015**, *141*, 285–292.
(112) Xie, Y.; Wang, J.; Xu, N.; Yu, S.; Zhang, M.; Huang, Z. *Energy Fuels*, **2014**, *28*, 3391–3398.
(113) Weng, W. B.; Wang, W.; He, Y.; Zhou, Y. J.; Zhou, J. H.; Cen, K. F. *Proc. Europ. Combust. Meeting,* 2013.
(114) Smith, G. P.; Golden, D. M.; Frenklach, Moriarty, N. W.; Eiteneer, B.; Goldenberg, M.; M.; Bowman, C. T.; Hanson, R. K.; Song, S.; Gardiner, W. C., Jr.; Lissianski, V. V.; Qin, Z., GRI-Mech 3.0., http://www.me.berkeley.edu/gri_mech/.
(115) Ranzi, E.; Sogaro, A.; Gaffuri, P.; Pennati, G.; Faravelli, T. *Combust. Sci. Technol.*, **2007**, *96*, 279–325.
(116) Varga, T.; Nagy, T.; Olm, C.; Zsély, I.; Pálvölgyi, R.; Valkó, É.; Vincze, G.; Cserháti, M.; Curran, H. J.; Turányi, T. *Proc. Combust. Inst.*, **2015**, *35*, 589–596.
(117) Turányi, T.; Nagy, T.; Zsély, I. G.; Cserháti, M.; Varga, T.; Szabó, B. T.; Sedyó, I.; Kiss, P. T.; Zempléni, A.; Curran, H. J. *Int. J. Chem. Kinet.*, **2012**, *44*, 284–302.
(118) Wang, H.; Sheen, D. A. *Prog. Energy Combust. Sci.*, **2015**, *47*, 1–31.
(119) Frenklach, M.; Packard, A.; Garcia-Donato, G.; Paulo, R.; Sacks, J. *SIAM/ASA J. Uncertainty Quantification*, **2016**, *4*, 875–901.
(120) You, X.; Russi, T.; Packard, A.; Frenklach, M. *Proc. Combust. Inst.*, **2011**, *33*, 509–516.
(121) Frenklach, M.; Li Kwok Cheong, C.K. LDV Measurements of Gas Flow Behind Reflected Shocks. In *Dynamics of Flames and Reactive Systems*; Soloukhin, R. I., Oppenheim, A. K., Bowen, J. R., Manson, N., Eds.; American Institute of Aeronautics and Astronautics: New York, 1985; pp 722–735.

(122) Frenklach, M.; Bornside, D. E. *Combustion and Flame*, **1984**, *56*, 1–27.
(123) Petersen, E. L.; Hanson, R. K. *Shock Waves*, **2001**, *10*, 405–420.
(124) Davidson, D. F.; Hanson, R. K. *WSSCI Fall Meeting.* University of California at Los Angeles, Los Angeles, CA, 2003.
(125) Petersen, E. L.; Rickard, M. J. A.; Crofton, M. W.; Abbey, E. D.; Traum, M. J.; Kalitan, D. M. *Meas. Sci. Technol.*, **2005**, *16*, 1716–1729.
(126) Dryer, F. L.; Chaos, M. *Combust. Flame*, **2008**, *152*, 293–299.
(127) Ihme, M. *Combust. Flame*, **2012**, *159*, 1592–1604.
(128) Urzay, J.; Kseib, N.; Davidson, D. F.; Iaccarino, G.; Hanson, R. K. *Combust. Flame*, **2014**, *161*, 1–15.
(129) Grogan, K. P.; Ihme, M. *Proc. Combust. Inst.*, **2015**, *35*, 2181–2189.
(130) Meyer, J. W.; Oppenheim, A. K. *Proc. Combust. Inst.*, **1971**, *13*, 1153–1164.
(131) Hughes, K. J.; Turányi, T.; Clague, A. R.; Pilling, M. J. *Int. J. Chem. Kinet.*, **2001**, *33*, 513–538.
(132) Ripley, D. L. *J. Chem. Phys.*, **1966**, *44*, 2285.
(133) Jachimowski, C. J.; Houghton, W. M. *Combust. Flame*, **1971**, *17*, 25–30.
(134) Karkach, S. P.; Osherov, V. I. *J. Chem. Phys.*, **1999**, *110*, 11918.
(135) Michael, J. V.; Sutherland, J. W.; Harding, L. B.; Wagner, A. F. *Proc. Combust. Inst.*, **2000**, *28*, 1471–1478.
(136) Ibraguimova, L. B.; Smekhov, G. D.; Shatalov, O. P. Comparative analysis of the rates of chemical reactions describing the combustion of hydrogen–oxygen mixtures. http://www.chemphys.edu.ru/media/files/2009-06-29-001_.pdf.
(137) Troe, J. *Proc. Combust. Inst.*, **2000**, *28*, 1463–1469.
(138) Michael, J. V.; Su, M.-C.; Sutherland, J. W.; Carroll, J. J.; Wagner, A. F. *J. Phys. Chem. A*, **2002**, *106*, 5297–5313.
(139) Bates, R. W.; Golden, D. M.; Hanson, R. K.; Bowman, C. T. *Phys. Chem. Chem. Phys.*, **2001**, *3*, 2337–2342.
(140) Fernandes, R. X.; Luther, K.; Troe, J.; Ushakov, V. G. *Phys. Chem. Chem. Phys.*, **2008**, *10*, 4313–4321.
(141) Sellevag, S. R.; Georgievskii, Y.; Miller, J. A. *J. Phys. Chem. A*, **2008**, *112*, 5085–5095.
(142) Cohen, N.; Westberg, K. R. *J. Phys. Chem. Ref. Data*, **1983**, *12*, 531.
(143) Tsang, W.; Hampson, R. F. *J. Phys. Chem. Ref. Data*, **1986**, *15*, 1087.
(144) Sharipov, A.; Starik, A. *J. Phys. Chem. A*, **2011**, *115*, 1795–1803.
(145) Koike, T. *Bull. Chem. Soc. Jpn.*, **1991**, *64*, 1726–1730.
(146) Thielen, K.; Roth, P. *Ber. Bunsenges. Phys. Chem.*, **1983**, *87*, 920–925.
(147) Rawlins, W. T.; Gardiner, W. C. *J. Phys. Chem.*, **1974**, *78*, 497–500.
(148) Christoffel, K. M.; Bowman, J. M. *J. Phys. Chem. A*, **2009**, *113*, 4138–4144.
(149) Friedrichs, G.; Herbon, J. T.; Davidson, D. F.; Hanson, R. K. *Phys. Chem. Chem. Phys.*, **2002**, *4*, 5778–5788.
(150) Troe, J.; Ushakov, V. *J. Phys. Chem. A*, **2007**, *111*, 6610–6614.
(151) Joshi, A. V.; Wang, H. *Int. J. Chem. Kinet.*, **2006**, *38*, 57–73.
(152) Li, J.; Wang, Y.; Jiang, B.; Ma, J.; Dawes, R.; Xie, D.; Bowman, J. M.; Guo, H. *J. Chem. Phys.*, **2012**, *136*, 041103.
(153) Colberg, M.; Friedrichs, G. *J. Phys. Chem. A*, **2006**, *110*, 160–170.
(154) Fassheber, N.; Friedrichs, G.; Marshall, P.; Glarborg, P. *J. Phys. Chem. A*, **2015**, *119*, 7305–7315.
(155) DeSain, J. D.; Jusinski, L. E.; Ho, A. D.; Taatjes, C. A. *Chem. Phys. Lett.*, **2001**, *347*, 79–86.
(156) Timonen, R. S.; Ratajczak, E.; Gutman, D. *J. Phys. Chem.*, **1988**, *92*, 651–655.
(157) Hsu, C.-C.; Mebel, A. M.; Lin, M. C. *J. Chem. Phys.*, **1996**, *105*, 2346.
(158) You, X.; Wang, H.; Goos, E.; Sung, C.-J.; Klippenstein, S. J. *J. Phys. Chem. A*, **2007**, *111*, 4031–4042.
(159) Mittal, G.; Sung, C. J.; Fairweather, M.; Tomlin, A. S.; Griffiths, J. F.; Hughes, K. J. *Proc. Combust. Inst.*, **2007**, *31*, 419–427.
(160) Timonen, R. S.; Ratajczak, E.; Gutman, D.; Wagner, A. F. *J. Phys. Chem.*, **1987**, *91*, 5325–5332.
(161) Krasnoperov, L. N.; Chesnokov, E. N.; Stark, H.; Ravishankara, A. R. *J. Phys. Chem. A*, **2004**, *108*, 11526–11536.
(162) Cribb, P. H.; Dove, J. E.; Yamazaki, S. *Combust. Flame*, **1992**, *88*, 169–185.

(163) Westmoreland, P. R.; Howard, J. B.; Longwell, J. P.; Dean, A. M. *AIChE J.*, **1986**, *32*, 1971–1979.
(164) Troe, J. *Proc. Combust. Inst.*, **1975**, *15*, 667–680.
(165) Jasper, A. W.; Dawes, R. *J. Chem. Phys.*, **2013**, *139*, 154313.
(166) Kathrotia, T.; Fikri, M.; Bozkurt, M.; Hartmann, M.; Riedel, U.; Schulz, C. *Combust. Flame*, **2010**, *157*, 1261–1273.
(167) Kee, R. J.; Rupley, F. M.; Miller, J. A. Chemkin-II; Report No. SAND89-8009B.
(168) Kintech Lab, Chemical Workbench, http://www.kintechlab.com/.
(169) Hegde, A.; Li, W.; Oreluk, J.; Packard, A.; Frenklach, M. *Consistency analysis for massively inconsistent datasets in Bound-to-Bound Data Collaboration*: in preparation.
(170) Manion, J. A.; McGivern, W. S. *Int. J. Chem. Kinet.,* **2016**, 48, 358-366.
(171) Boyd, S.; Vandenberghe, L. *Convex Optimization*, Cambridge University Press, Cambridge, UK, 2004.
(172) Yates, D. R.; Li, W.; Westmoreland, P. R.; Speight, W.; Russi, T.; Packard, A.; Frenklach, M. *Proc. Combust. Inst.* **2015**, *35*, 597-605.
(173) Egolfopoulos, F. N.; Hansen, N.; Ju, Y.; Kohse-Höinghaus, K.; Law, C. K.; Qi, F. *Prog. Energy Combust. Sci.* **2014**, *43*, 36-67.
(174) Frenklach, M. in *Combustion Chemistry* (W. C. Gardiner, Jr., Ed.) Springer-Verlag, New York, 1984, pp. 423–453.